Review

Material jetting for advanced applications: A state-of-the-art review, gaps and future directions

Ahmed Elkaseer [a,b,c,*], Karin J. Chen [a], Jan C. Janhsen [d], Oliver Refle [d], Veit Hagenmeyer [a], Steffen G. Scholz [a,b]

[a] *Institute for Automation and Applied Informatics, Karlsruhe Institute of Technology, Hermann-von-Helmholtz-Platz 1, 76344 Eggenstein-Leopoldshafen, Germany*
[b] *Karlsruhe Nano Micro Facility, Karlsruhe Institute of Technology, Hermann-von-Helmholtz-Platz 1, 76344 Eggenstein-Leopoldshafen, Germany*
[c] *Faculty of Engineering, Port Said University, Port Fouad 42526, Egypt*
[d] *Department of Additive Manufacturing, Fraunhofer Institute for Manufacturing Engineering and Automation, Nobelstrasse 12, 70569 Stuttgart, Germany*

A B S T R A C T

The proven ability of additive manufacturing (AM, also known as 3D printing) to fabricate complex components with substantial reductions in material wastage and reduced lead times has made it a key enabling technology for numerous important industrial applications. Of current AM processes, material jetting (MJ) is demonstrating considerable potential for producing multi-material, intricate, 3D components and systems with integrated functionality, with the additional benefit that the process can be easily integrated with other manufacturing procedures. However, material jetting of functional materials to produce advanced applications still poses numerous technological challenges which hinder its full industrial exploitation. These extend from the limited range of high-performance materials with consistent properties usable for MJ, through the need to enhance the process itself by optimizing the droplet formation process, tuning waveforms for specific processes, modification of substrate and substrate/jetted material interactions, the complexities of curing and post-processing procedures, and the challenge of characterizing the 3D printed parts. In this context, this article attempts to provide a comprehensive discussion of the principles and characteristics of the most recent material jetting technology and reviews the state-of-the-art research and development being conducted. This review identifies existing gaps with regards to high-performance UV-curable inks, printing behavior of non-Newtonian fluids, optimum jetting and curing strategies and effective measures for achieving high-precision MJ. Future work should bridge the aforementioned gaps in order to improve the performance of the technology, thereby making it more attractive for large-scale adoption by industry and increasing market acceptance and penetration of material jetting for advanced applications.

1. Introduction

Material jetting (MJ) is a key enabling and competitive manufacturing technique for a broad range of industrial and scientific applications due to its cost-effectiveness, high-throughput and scalability of production, along with its ability to extend functionality via multi-material printing [1–3]. However, MJ exceeds competing additive manufacturing (AM) processes such as material extrusion, binder jetting or powder bed fusion in precision and scale of surface texture of printed parts achievable [4]. MJ generates 3D parts based on the ink jetting

technology, and thus it is also commonly referred to as 3D inkjet printing or direct inkjet printing.

MJ technology possesses huge potential to additively manufacture miniaturized and complex systems because of its ability to print multiple functional materials in a high-resolution manner, for instance microsystems based on dielectric and conductive inks with electronics embedded during the manufacturing process [5], or miniature 3D printed metallic pillars [6] and 3D printed optical lenses [7]. MJ possesses a huge potential when it comes to functionally graded materials, that is mixing two base materials in a voxel-like manner [8] to

---

selectively generate finely tuned properties within a part such as dielectric [9] or bio-inspired soft to hard properties [10].

The currently commercially available MJ printers generate 3D objects based on two steps: (1) printing/jetting and (2) curing. During the printing step printheads eject tiny and precise drops of ink via a number of nozzles onto a substrate, where the droplets dispense and coalesce. Inkjet printing (IJP) can be, in general, classified into two groups in terms of jetting technology; continuous inkjet (CIJ) printing and drop-on-demand (DoD) printing. The CIJ printing is characterized by a continuous stream of droplets being ejected, while in DoD printing, an applied signal waveform whether thermal or piezoelectric, allows for the ejection of droplets at high frequency only when demanded [11], see Fig. 1 illustrating DoD inkjet printing.

In MJ, the printer jets at least two materials: build material and support material. The latter material supports overhanging features and will be immersed after printing in a solution to dissolve the support material. Some systems such as PolyJet by Stratasys [12] or MultiJet Printing by 3D Systems [13] apply an additional layer levelling step before the curing. However it should be noticed that PolyJet and MultiJet Printing are trademarks, both describing the MJ technology, which is the official term according to the latest standard on additive manufacturing ISO/ASTM 52900:2021 [14]. The layer levelling step is usually applied in order to take off protruding material from the printed and yet uncured layer, ensuring that the surface is smoothen and that the resulting layer height meets the target layer height. This step is then followed by a UV-curing step solidifying this printed layer [15]. These steps are going to be repeated layer-by-layer until the 3D object is completed.

So far, and based on a recent review by Gülcan et al. the main target applications of parts printed on commercial MJ printers are restricted to color models and applications that are not subject to heavy loads such as moulds or for prototyping purposes. This can be explained by the inherently low mechanical and thermal performance of the commercially available photopolymer inks [16]. Current UV-curable materials are also limited in durability due to long-term aging and mechanical degradation caused by the exposure to light and humidity [17]. Fig. 2 shows the tensile strength and heat deflection temperature of various commercial polymer materials used in AM [18–24]. Commercial inks for MJ are so far still restricted to the lower tensile strength region and heat deflection temperature [21,22], while materials used for vat photopolymerization (VPP) on the contrary covers a much wider range of mechanical and thermal properties [18–20]. Especially the hot vat photopolymerization (Hot Lithography) technology can process materials suitable for high temperature applications [18]. Thermoplast can even span a wider material range as it cannot only print ABS but also PEEK [23–25]. Based on this Figure, it can be clearly seen that inks used for MJ cannot compete with thermosets printed with VPP and thermoplastic materials, yet.

Nevertheless, the combination of MJ's strength in high-resolution and multi-material printing of functional materials facilitates highly
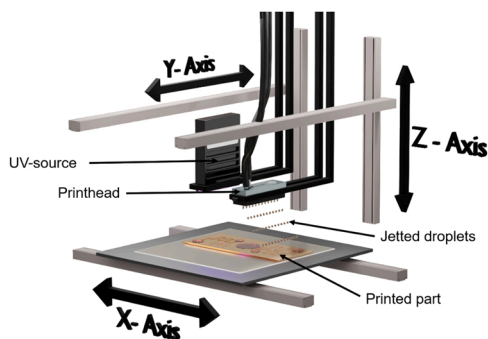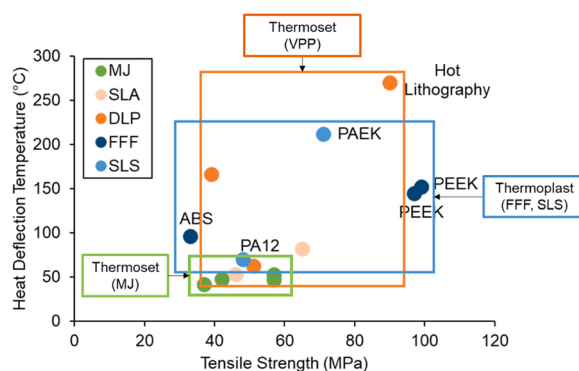

Fig. 2. Mechanical and thermal properties of various plastic materials used for various additive manufacturing technologies (material jetting (MJ), stereo-lithography (SLA), digital light processing (DLP), fused filament fabrication (FFF) and selective laser sintering (SLS)).

advanced applications. For example, microfluidic systems equipped with sensors, evaluation electronics, solar cells and/or battery [26–28], or pacemakers for heart and brain stimulation, low-cost wearable sensors for patient monitoring, tailored pills or functionalized biointerfaces on implants [29–31] could all be printed in a single print job. Further applications, which are not reported yet, could be self-guiding drug delivery pills, pills with diagnostic functions, smart contact lenses with augmented reality or small intelligent sensors with data processing function for telemedicine. New materials, such as photothermal nanocomposite [32], could be used for self-heating patches. MJ could also offer the possibility to incorporate functional structures that can trigger an alarm in the case of an almost complete failure or when the wear goes beyond a critical level [33]. Importantly, MJ provides a basis for 4D printing in which the structural response in time is controlled while creating the geometry of the printed component. 4D printing enables parts with a pre-programmed transient response (e.g., folding, deployment, sensing, etc.), that manifests after printing. In 4D printing, components with smart, predictable and time variant shape/property/functionality can be produced. Tailoring and controlling behavior of printed parts in this manner could enable self-assembly, self-sensing, multi-functionality, and self-repair.

In order to enable these above-mentioned applications, the MJ printing process must be well understood in order to control it well, also to further increase the performance, both of the production and the printing, as the printing quality affects the performance of the functional structures. By pushing the boundaries of the current state-of-the-art of MJ, future industrial demands for a wide range of applications can be fulfilled [11]. MJ may seem simple but, in fact, many and varied skills and a code of restrictive practice are necessary to achieve satisfactory results due to the numerous challenges inherent in the technology [15] and the interdependence of the complex steps involved in the MJ process chain. Examples of the technical and technological issues to be considered for successful implementation of the process are e.g., the limited range of enhanced inks with integrated functionality, making it a challenge to select an ink that embodies the desirable characteristics in terms of the physical and chemical requirements. Moreover, the complex nature of the process chain of material jetting for generating 3D parts with given characteristics, which includes a highly dynamic droplet generation, the need for optimized waveforms to jet the inks, the complex interaction between droplets and substrate, intricate curing and post-processing procedures, process compatibility between multiple materials, as well as the challenge of characterizing the functionality of printed parts are issues to be addressed. Several research studies have attempted to investigate a number of the above-mentioned challenges, but a comprehensive review of the current state-of-the-art of the material jetting technology is still not available. In this context, this paper aims to provide a systematic review of the current state-of-the-art of

Fig. 1. Schematic of the DoD inkjet printing technology, where the printhead jets UV-curable droplets which will be cured by the UV-source.

material jetting for advanced applications in order to identify existing gaps and give insights into recommendation for future directions.

The remainder of the paper is organized as follows. The first part of this review paper (Sections 2 – 5) guides the reader through the relevant topics of jetting process from jettable inks to droplets/substrate interaction. Then Section 6 explores the curing process and gives a compact overview on various photocuring mechanism and introduces the model for the assessment of the cure depth. In addition, the state-of-the-art curing strategies reported for MJ are presented as well. Section 7 provides an overview of quality issues in material jetting (3D printing) such as shrinkage, layer height inconsistency and surface unevenness, oxygen inhibition and gas dissolvement in liquids. Moreover, state-of-the-art quality assuring measures to combat some of these issues are reviewed. The next Section provides numerous applications of material jetting technology. After that, the review paper briefly summarizes the existing gaps and scientific challenges and recommends future works. Finally, the Section "Conclusions" provides insights gained out of the conducted review.

2. Jettable inks

Inkjet inks can be in general categorized in terms of their carrier fluids into phase-change (also called hot-melt), water-based, solvent-based, oil-based and UV-curable inks [15,34]. Hybrid inkjet inks contain, as suggested by the name, more than one type of carrier, for instance water-based UV-curable inkjet inks which require the solvent to be removed before UV-curing [34]. Among these ink types, UV-curable inks and solvent-based nanoparticle-loaded conductive inks are most commonly reported in the literature. Solvent-based conductive ink activates its conduction after drying and sintering. In particular, the drying removes remaining solvent of the liquid and the sintering at even higher temperature thermally decomposes the non-conductive outer shell on each metallic nanoparticle to facilitate the agglomeration of the nanoparticles [35,36].

UV-curable inks have been widely used for industrial applications such as coating, package decoration and labelling [15,37,38]. Although UV-curable inks are deemed safe for the operator and environment, as it does not contain any solvents, the application of UV-curable inks for food packages is limited, because harmful low-molecular weight acrylic monomers, photoinitiators and photolytic decomposition products migrate through the substrate and eventually get ingested by being in contact with the food [39–41]. In terms of biocompatibility, some studies demonstrated that compounds released from 3D printed orthodontic devices based on photopolymer dental resin can cause cytotoxicity, mucosal irritation, genotoxicity and allergic reaction [42–44]. Further research in non-toxic photoinitiators and monomers are therefore recommended to widen the range of applications. UV-curable inks are easy to handle as they do not dry in the print system, enabling better nozzle stability compared to volatile solvent-based or water-based inks [37].

The products based on UV-curable inks often offer higher opacity, coverage, scratch and chemical resistance [37]. UV-ink's volatile organic compounds (VOC) emissions are near zero level and hence UV-inks are considered safer for the operators and environment. Moreover, curing UV-inks requires less energy as no solvents or water ought to be evaporated from the ink. UV-curable inks are therefore suitable for building up three-dimensional structures, as it is considered a nearly 100% solid system. Another major advantage of UV-curing inks compared to the thermal curing ones is the ability to use heat-sensitive substrates since the UV-curing does not damage the substrates [45–47]. In addition, the curing of UV-sensitive inks consumes less energy, takes place faster and requires less space compared to thermally-cured inks [3–6]. From a process control point of view, the UV-curing process can be controlled more precisely as UV-lamps and the photochemical process can be switched on and off instantaneously. The photoinduced curing process allows more distinct and flexible control over the

cross-linking process according to the required structure resolution by tuning parameters such as intensity, wavelength and spatial distribution [45]. As formally mentioned, low-viscous inkjet inks have inherently low mechanical and thermal properties due to the use of low-weighted polymers [48]. To increase the mechanical properties of inkjet-printed parts, it would be beneficiary to increase the polymer load or to incorporate particles, which however, go along with the increase of viscosity of the ink. Hence, further research is not only needed in developing high-performance inks but also in introducing jetting devices/printhead systems for printing high-viscous fluids efficiently.

With material jetting being a promising technology to enable cost-efficient and precise production of complex structures, there is a high demand for functional inks. Various materials for inkjet printing based on UV-curing equipped with functionality were explored in the literature. Investigations into electromagnetic responsive ink consisting of iron oxide nanoparticles within a UV-curable matrix resin had been conducted [49]. Several works with dielectric inkjet inks have been reported as well [9,50]. Saleh et al. inkjet-printed a checkered pattern of carbon black ink and UV-curable monomer and tailored the dielectric properties of this composite layer by varying the ratio of the carbon ink and polymer [49]. Inkjet printing can also process UV-curable ceramic inkjet inks formulated from UV-curable monomers, photoinitiators and ceramic pigments. These type of inks do not require a very high temperature post-processing step for removing organics and sintering as opposed to conventional ceramic material [51].

3. Characterization of jettable inks

It is advisable to characterize potential inks before processing them in the printhead, thus in this following Section the most important methods to assess the jettability of inkjet inks including suitable measurement equipment are summarized.

Dimensionless groupings such as the Reynolds number (Re) and Weber number (We) have been derived using ink governing properties, namely viscosity, surface tension, density and velocity, which dominate the jetting performance of a processed ink. Ohnesorge number (Oh) has been used to determine the feasibility of the ink [52–54]. Oh number is defined by Eq. 1 as follows

$$Oh = \frac{\sqrt{We}}{Re} = \frac{\eta}{\sqrt{(\sigma \rho a)}} \tag{1}$$

where ρ, σ and η are the density, the surface tension and the dynamic viscosity of the inkjet fluid respectively, and a is a characteristic length which is typically the diameter of the nozzle, drop or the jet. The Ohnesorge number is calculated as function of the Reynolds number Re (the ratio between inertial and viscous forces in a moving fluid) and the Weber number (We) which is the ratio between inertia and surface tension, and does not depend on the drop velocity. When Re is too low, the actuation is unlikely to produce droplets, i.e., to execute droplet pinch-off from the oscillating meniscus. In contrast, if the Re is too high, the droplet would splash over the substrate, which is undesirable for precision printing. When Oh is too large, the ink is too viscous to be jetted through pressure buildup, but when Oh is too small, the surface tension is strong enough to cause satellite droplet formation due to the Plateau-Rayleigh instability of the ink filament, which is also undesirable in controlled inkjet printing [19]. As temperature decreases, the viscosity and surface tension increase, which leads to a higher Oh value. Kang's experiments [55] showed that cooling the ink's temperature can stabilize ink drop and avoid formation of satellites drops. The Z number, which is the inverse of Oh number (Eq. 2) is, however, more often used in the literature [53].

$$Z = \frac{1}{Oh} \tag{2}$$

Fromm first proposed the working condition of $Z > 2$ for stable drop

generation [52]. Reis & Derby later defined boundary conditions of $10 > Z > 1$ based on the results from a numerical simulation of drop formation for proper jetting behavior [56]. Jang et al. redefined the printable range as $14 > Z > 4$ taking the minimum stand-off distance, the maximum jetting frequency and the positional accuracy into consideration [57]. The above-mentioned thresholds can be used for the first assessment of whether an ink is printable on most printheads, but it should be noted that the current development is pointing at expanding the printing range, so that more functional inks, such as high-viscous inks can be jetted as well (Fig. 3).

Despite fitting into the printable regime, the Weber number must also be considered, because sufficient energy is required to overcome the fluid/air interface tension at the nozzle. Derby therefore suggested a minimum Weber number of $We > 4$ for proper drop formation [53]. On the contrary, if the Weber number is too high, an onset of splashing of the ink on the substrate takes place [58]. Fiona et al. explored the effect of surface roughness and wettability on the splashing limit of blood droplets, a non-Newtonian colloidal fluid. In comparison to wettability, they discovered that roughness has a significant influence on the splashing/non-splashing behavior threshold [59]. Few studies investigated the drop impact of non-Newtonian viscoelastic fluids and compared their performance with the behavior of Newtonian fluids as well [60,61], although Jung and Hoath didn't conclude any interdependence between the high-shear rheological properties of the fluid and the droplet impact [60], while Son and Kim observed a different impact during the receding phase [61]. Considering that the market has recently seen the emergence of advanced facilities capable of jetting higher-viscous inks, a lack of understanding of the new printing region and the droplet impact behavior of high-viscous inks with viscoelastic properties remains.

As previously stated, the Ohnesorge number is calculated from the viscosity, density and surface tension of the ink. Rotational rheometer is commonly used for measuring the shear viscosities of inkjet inks [56,57,62–64]. A rotational rheometer operates with two rotating elements between which the fluid to be investigated is sandwiched and sheared. In case of Newtonian ink behavior, which applies to many low-viscous inkjet inks, measurements at lower shear rate are sufficient, as the viscosity does not depend on the shear rate [53]. The extensional viscosity for Newtonian fluids is approximately 3 times the shear viscosity [65]. In order to observe any shear rate dependent properties of the ink, shear rates close to the ones in a piezo inkjet printhead, that is 10^5 s^{-1} [66] or even 10^6 s^{-1} [34], should be considered as well. Higher shear viscosity measurements can be performed on a capillary rheometer [67],

microfluidic sensor-based viscometer [68] or a multi-pass rheometer [69]. The latter one enables shear rates up to 160,000 s^{-1} and therefore allows measurement at shear rates similar to inkjet printing [69]. The filament thinning and break-up behavior of inkjet inks can be observed with the help of an extensional rheometer named "Cambridge Trimaster" which records the stretching and thinning process of fluid between two rapidly opposing moving pistons with a high-speed camera [70].

Several studies found out that inks with even a slight amount of polymer molecule, particle or pigment load deviate from the Newtonian fluid behavior, especially at high shear rates [62,71]. Shear-thinning flow behavior is for example characteristic of concentrated suspension [63]. Further examples of non-Newtonian inks are given in the review paper of Siacor et al. [72]. Non-Newtonian fluids obviously behave differently from Newtonian inks. Du et al. proposed a new range within which a stable single droplet formation based on the dimensionless numbers Weissenberg (Wi), Ohnesorge number and Reynolds number can be achieved for polymer loaded inks [62]. Further dimensionless numbers describing the material property of viscoelastic inks are Deborah number, elasto-capillary number [73] and elasticity number [74]. A deep investigation into the printability thresholds, similar to the printing region proposed by Derby, of viscoelastic fluids taken into consideration new dimensionless numbers should be done. Other devices for gauging the viscoelastic effect at high shear rates are for example dynamic squeeze flow rheometer, also named piezo axial vibrator (PAV), which performs measurements at frequencies from 0.1 s^{-1} to 4000 s^{-1} [75], and a light scattering based micro-rheometer called diffusing wave spectroscopy (DWS), measuring at frequencies at the order of 10^6 [76].

For calculating the Ohnesorge number it is required to know the dynamic surface tension as well. Surface tension determines the drop formation, the jetting stability and the wettability of the ink on the substrate [77]. The static value, the equilibrium state of the surface tension, can be determined by classical methods such as Du Noüy ring or Wilhelmy plate method [78]. However, all interfaces in inkjet printing are created within the order of few microseconds to milliseconds [77], which is why the dynamic surface tension is more accurate to assess the ink behavior. One way to obtain the surface tension for short interface ages under one second is the maximum bubble pressure method [64,77,79–81]. In this method, a capillary is immersed into the liquid through which a gas flow is conducted so that a bubble grows at the tip of the capillary [82]. The surface tension is calculated based on the Young-Laplace equation and the measured maximum pressure within the bubble p_b (Eq. 3), which the bubble reaches when taking the shape of a hemisphere, and the bubble curvature r which is identical to the capillary radius at maximum pressure.

$$\sigma = \frac{p_b * r}{2} \tag{3}$$

The surface age refers to the time between the beginning of the bubble formation and the maximum pressure. By varying the speed at which bubbles are formed, different surface ages can be set [81] (Fig. 4).

The shorter the bubble surface age, the higher the surface tension [77]. The higher the surface tension, the closer it is to the static surface tension value as the surfactants have enough time to align along the liquid/gas interface of the bubble and reaching an equilibrium state [81]. Zhou et al. proposed a high-throughput screening method by using a head with multiple pipettes which performs measurements of viscosity and surface tension of multiple liquids at once, hence, speeding up the search for an ideal formulation of inkjet ink [83]. Typical operating window for viscosity and surface tension of most piezo-based drop-on-demand printheads is 5 mPa•s to 40 mPa•s and 20 mN/m to 40 mN/m, respectively [34].

The overview in this Section clearly shows that measurement devices for the rheological characterization of inkjet inks has been steadily developed in order to reach the time scales relevant for inkjet printing.
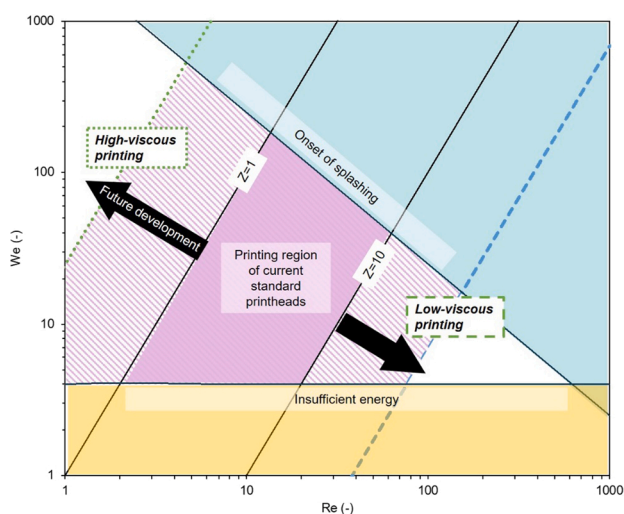

Fig. 3. Printing region of current standard printheads and the future direction of development of functional inkjet printing.
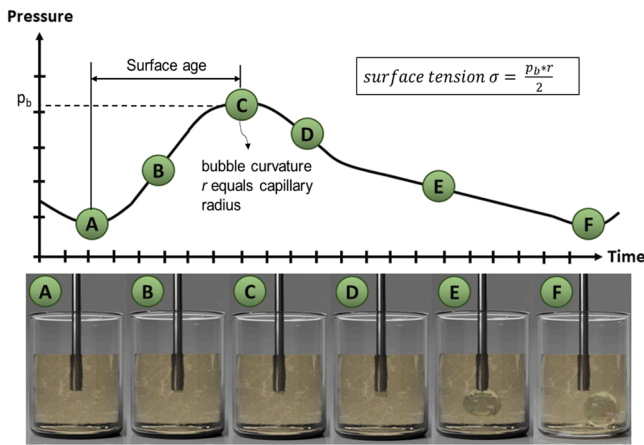Adapted from illustration reported in [56].

Fig. 4. The course of the bubble pressure during one measurement with the maximum bubble pressure method. The surface tension is calculated based on the maximum bubble pressure reached when the bubble curvature equals the capillary radius.

Although inkjet printing has been used in the printing industry for decades, standards or widely accepted guidelines on how to conduct rheological characterization of functional inkjet inks do not exist. Hence, it is recommended to establish standards on how to test functional inkjet inks, so that in future inkjet ink specifications are transparent and comparable for the users.

4. Drops generation

The quality of parts printed by MJ is strongly affected by the characteristics of the droplets generated from the printhead. In this Section the formation of droplets of both Newtonian and non-Newtonian fluids is briefly explained. The second part demonstrates the importance of the waveform on the jetting and printing quality. The focus of this paper will be given to the piezoelectric-based DoD printing mode.

As previously stated, two different jetting mechanisms can be utilized in the inkjet process. First and more conventional is the continuous inkjet printing (CIP) mode in which a continuous stream of droplets is dispensed through the nozzle followed by the application of Rayleigh instability principle to separate the jetted stream into droplets [84]. Second and more advanced is the drop-on-demand (DoD) printing technique in which droplets are controlled and jetted only when needed via thermal or digital piezoelectric signal [85]. Piezo-based inkjet printing describes a printhead in which an electric voltage signal is provided to the piezoelectric transducer to activate the ejection in piezoelectric DoD printing [86]. The ink in the nozzle is first extruded and pushed out of the nozzle when the piezoelectric actuation deforms (Fig. 5 (1)). A short time later, the liquid flow rate lowers, and the velocity differential between the drop head and tail lengthens the liquid column (2). As additional surfaces are produced, the extension rate drops, but the surface energy increases. The tail then disintegrates at the nozzle exit, resulting in a free liquid thread with a bulbous head (3). Recoil happens when two ends react differently and the surface contracts asymmetrically. With the contraction of the liquid thread, a second break-up occurs between the liquid thread and the head (4). Finally, the two droplets recombine to produce a big droplet when the trailing droplet velocity is higher than the main droplet velocity (5). After oscillation, a single droplet in an equilibrium state is created (6) [87–89].

However, the elongated liquid thread can be divided into the leading drop and some smaller satellite drops by instability mechanisms as well (Fig. 6) [90].

The visual observation of drop falling behavior can be acquired from camera of the dropwatcher, which provides accurate measurements of
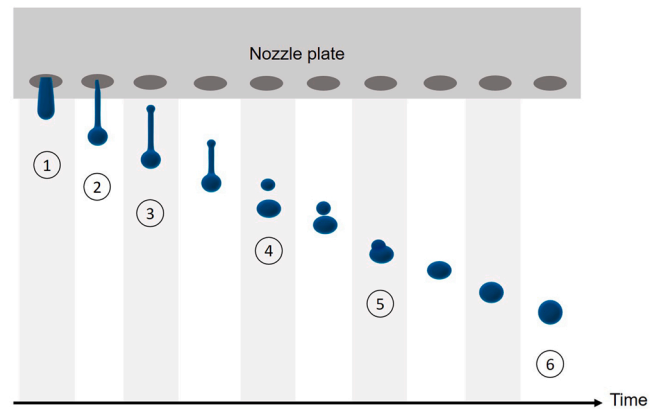

Fig. 5. Droplet formation of a Newtonian fluid in DoD piezo inkjet printing. The final stable droplet is created upon the merging of the secondary droplet with the main droplet.

Fig. 6. Satellite drops in inkjet printing. The main droplet is followed by multiple smaller droplets.

drop volume, drop shape, and drop velocity.

Due to the trend towards more functional inkjet inks, complex fluids with non-Newtonian behavior are gaining more attention. Polymer loaded inks [62] or bioinks [73] are reported to not behave like a Newtonian fluid but show considerably viscoelastic properties caused by the entanglement of long polymer molecules [91]. Obviously, the droplet formation and drop impact of these non-Newtonian inks differ from Newtonian inks. The higher the polymer concentration or the molecular weight of the polymer, the greater the breakup length of the thread of a jet [62,92,93] and the higher the time to separation for the primary drop [92] (Fig. 7). Furthermore, a larger voltage pulse is required to form a droplet and the velocity of the primary drop decreases the higher the polymer concentration in the fluid is [92,94]. One positive side-effect of adding polymer is the suppressing of satellite droplets, as the trail droplet is either pulled back to the nozzle or the primary droplet is connected by a thin thread, and therefore not breaking up [92, 93]. If the polymer concentration is increased above a particular threshold, the droplet is not able to pinch-off from the nozzle [95].

To produce exact printing results, the collaboration of several factors is critical, e.g., ink properties, waveform, conditions of substrate, nozzle geometry, and so on [96]. Nevertheless, the actuation waveform is the key element in the current study, since many studies suggest that the driving waveform has strong influences on the droplet formation, velocity and drop size [85,97,98]. Furthermore, the electric voltage signal's waveform, driving voltage, and pulse interval can all be adjusted to generate different drop ejection patterns [99]. In order to advance the knowledge about the effects of the waveform in DoD printing, and to
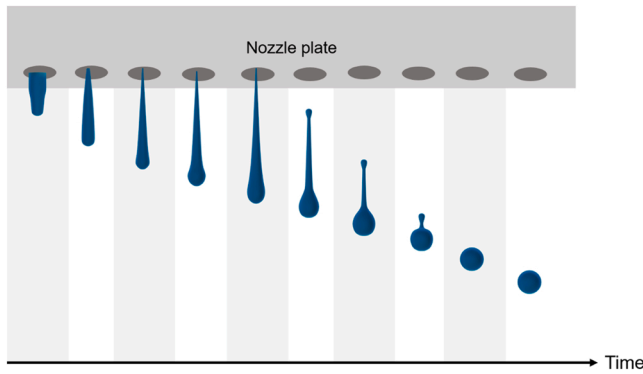
Fig. 7. Droplet formation of a viscoelastic fluid in DoD piezo inkjet printing. Due to the elastic effect a separation of the tail into two droplets does not happen therefore preventing the emergence of satellite drops.

identify the optimal operating parameters for droplet generation, Aqeel et al. [100] studied two different types of waveforms, namely the unipolar and bipolar actuations, with different combinations of time duration for the push action, pull action and time between the push and pull as well as the amplitude of the waveform. Their results showed that the radius of droplet can be as small as about 40% of the nozzle orifice radius and the bipolar waveform showed more advantages over the unipolar ones regarding faster and stable droplet formation.

To achieve the patterns with finer features it is necessary to generate smaller sized droplets while using a standard printhead. In Duineveld's paper it has shown experimentally and theoretically that such droplets can be made via higher-order oscillatory meniscus modes [101]. Snyder et al. suggest an automatic waveform tuning methods for high-order waveform [102]. The fluid motion is restricted to the extremely near vicinity of the meniscus in this mode. When the printhead and pulse are tuned in such a way that an overtone of the waveguide coincides with a symmetric resonance mode of the meniscus, stable droplets more than an order of magnitude smaller than the usual droplet can be produced.

For better performance of printhead, not only small and stable droplet formation but also faster flying velocity is critical in commercial use. The systematic numerical simulations with special efforts on optimizing the contracting angle of the nozzle, the wettability of the inner surface conducted by Aqeel et al. [103] suggested that a small contraction angle causes satellite droplets while a large contraction angle reduces the droplet velocity. It was found that for a Newtonian liquid, the nozzle with contracting angle of 45° has relatively good printing quality and high-throughput printing rate.

Combining a high droplet velocity with a high jetting frequency namely droplet generation frequency is another effective technique to increase output rate for both industrial and scientific applications. However, frequency of jetting is really restricted by fluid dynamical instabilities that can occur near the nozzle's edge, where the flow within the nozzle interacts with the flow on the nozzle plate. As they affect the fluid dynamics of the oscillating meniscus, the nozzle shape and wetting qualities of the nozzle plate are critical for obtaining optimum stability [54]. In simulation conducted by Miers et al. [104] it appeared that only when the ejection velocity reaches certain extent, droplet generation can occur at the higher frequency of the driving signal. Furthermore, in contrast to commercial DoD inkjet frequency (~10 kHz) the simulation results suggest that droplet generation with nozzle size of 5 μm diameter under frequency of 1 MHz or even 2.5 MHz can be achieved, which can potentially boost productivity by at least 100 times. However, it needs to be emphasized that the deformation of droplet has been observed as well due to the large influence of the air's inertial force. Meanwhile, the overall velocity change of a falling drop varies with the frequency. The droplets with shorter interval have higher velocity than the general terminal velocity based on terminal velocity theory, which has taken the gravitational force, drag force and buoyancy into consideration, due to

the wake field of the former droplet and decreased drag force [105].

Even though the droplets have been successfully ejected and formed as designed, the whole droplet formation process sometimes can still be harmed by the entrainment of an air bubble [106]. The entrained air bubble disrupts or even completely stops the jetting process, resulting in a significant reduction in print quality and dependability. After jetting a droplet, the meniscus retracts inside the nozzle and a bubble pinch off when the meniscus motion reverses from inward to outward, away from the ink channel. According to the study by Fraters et al., the meniscus's center part travels inward while the outside region goes outward. As a consequence, an air cavity develops, which finally closes, squeezing the air bubble [107]. Therefore, the waveform design has huge impact on quality and quantity of inkjet printing. It is worth investigating the design processes of waveform design to efficiently attain suitable parameters [108]. In addition to the piezoelectric driving properties, it was found that impurities in the ink can trigger bubble nucleation as well [109]. Therefore, the other crucial elements need to be considered for a precise and reproductive printing result, e.g., liquid properties [110, 111] and substrate's condition. To avoid the appearance of undesired satellite droplets, the deformation of droplets and the formation of tail satellite droplets were investigated experimentally [112,113]. The critical criterion for formation of tail satellite droplets was proposed and the formation of satellite drops can be successfully predicted with theoretical recoil and pinch-off times.

In general, as yet, no well-defined methods for identifying optimal waveforms as a function of the ink's rheological properties and print-head parameters have been proposed. It is therefore recommended to develop a systematic approach that correlates printhead acoustic properties and the rheological properties of the inks in order to accelerate the determination of optimal waveforms for jetting newly developed inks. Looking at the above-reviewed literature one can argue that tuning waveforms need to be further investigated and may be automatized by utilizing artificial intelligence (AI) and a smart dropwatcher to characterize droplet generation under a wide range of jetting parameters. In addition, the interdependence of printhead geometry, printhead acoustic properties, meniscus pressure, particle load, ink recirculation and air degassing on jetting stability require further investigation. The search for an optimum setting of the printhead and the peripheral can be accelerated by establishing a simulation tool, which takes the above-mentioned aspects into account.

5. Droplet/substrate interaction

To begin with, it should be noted that in this Section, the term "substrate" is not only limited to the material, which carries the printed part, but should be extended to the previous printed layer as well, on which the liquid droplet is deposited. The interaction between the liquid droplet and each previous layer (wetting) predominantly influences the print quality in MJ in terms of achievable resolution and geometrical accuracy due to the layer-by-layer production of a 3D part. The wetting condition is defined by the contact angle between the droplet and substrate which depends on the substrate's surface energy and surface tension of the liquid. The surface quality, that is for instance surface roughness and contaminations, should be considered as well. Once the droplet touches a substrate, the features of the substrate begin to influence the droplet's behavior, such as splashing [59], coalescence, or spreading [114]. For various applications of printed items, several substrates with varying degrees of mechanical stability, conductivity, and wettability could be employed, such as paper-based substrate [115, 116], glass [117,118], PET substrate [119,120] or textiles [121,122]. However, no publications investigated the wetting behavior of printed droplets on inkjet-printed layers so far, although it is important to assess if the degree of curing and print settings such as surface temperature or print resolution affect the resulting print quality.

Via surface modification of substrates the desired patterns and printing results can be achieved [123,124]. Various experiments suggest

that plasma treatment can be used to improve the wettability of the substrate and to obtain proper ink adhesion to the substrate by increasing surface energy [125,126]. Orazbayev et al., by contrast, generated a hydrophobic coating by means of plasma treatment [127]. Park et al. pre-treated a hydrophobic coating with plasma selectively and observed that by controlling the plasma treatment time the wettability and therefore the droplet spreading diameter of the ink can be controlled [128]. The functionalized surface of a plasma-treated substrate diminishes over time [129] and depends on various process parameters such as treatment time or gas [130]. Other methods for modification, such as surface roughening and abrasive, liquid chemical processes can be used to treat polymer surfaces as well [131]. However, various materials exhibit varying degrees of resistance to treatment and need differing levels of treatment power. Additionally, they are influenced by environmental factors such as temperature and humidity.

Surface adhesion is highly associated not only with the surface energy but can also be negatively affected by contaminants, particles, and even fingerprints [132,133]. Mechanical practices such as grinding and polishing, and chemical pre-treatments like wiping and rinsing with solvents, and cleaners are common to pre-treat the surface of the substrate for printing and coating applications [134]. Plasma-treatment can also remove contaminations from the surface [135] which is a crucial step if a reproducible and robust printing process is to be established. Overall, plasma surface treatment is a suitable method, as one of the dry chemical techniques, to precisely control droplet/substrate interaction as it is environmentally friendly and can treat large number of materials including polymer-based, ceramics and metals without causing any morphologic alteration [136–138]. Yet, it is to investigate how surface can be selectively treated in multi-material inkjet-based 3D printing and how surface treatment can be incorporated into the printing process between the printing of each layer. Another major key research topic is to improve accuracy of the planes perpendicular to the printing platform which becomes crucial when cavities with high aspect ratios are to be printed and if no support material ought to be used.

6. Curing process

A crucial process step in MJ is curing which has a huge impact on the geometrical accuracy and the mechanical behavior of the printed part. Since UV-sensitive ink plays a major role in MJ, a detailed overview on the photopolymerization process as well as the model for determining curing depth is given in this Section. Furthermore, the curing strategy applied in MJ is explained.

6.1. Photopolymerization

An UV-curable ink is a mixture of photoinitiators, monomers, oligomers and other additives such as pigments, stabilizers, plasticizing agents and performance enhancing substances [139]. Curing is a term used to describe the process of polymer chain growth via monomers crosslinking that comes with a rise in the viscosity of the system until the material is solidified. The photoinduced chain growth is enabled either by free radicals (free-radical polymerization) [140], cations (cationic photoinduced polymerization) [141,142] or anions (anionic photoinduced polymerization) [143], whereby the latter one is rarely used due to the lack of commercially available photoinitiators [45]. The majority of commercially available UV-curable inks for MJ are based on acrylate monomers [144–149]. Main advantages of free-radical polymerization are the broad choice of design due to a wide selection of usable monomers [46,47,150], fast reaction [47], lower cost compared to cationic formulation [47,150] and its relative insensitivity to trace impurities [151]. Free-radical ink usually faces problems such as oxygen inhibition, polymerization induced shrinkage and subsequent stress development and unreacted monomer and photoinitiators can form dangerous and irritating byproduct [45]. Cationic photoinduced polymerization results in lower volume shrinkage and is insensitive to oxygen [47,152],

although it can be affected by moisture instead [47,150]. Its capability to "dark cure" after being exposed to UV-light, which means further passive curing for a long time without additional UV irradiation, can be useful if it comes to curing thick layers, colored or filled polymer system in order to complete conversion [45,47,152]. Atsushi et al. developed a cationic polymer ink that enables higher curing speed at lower curing energy while having better adhesion compared to the radical ink investigated in the same study [150]. While cationic and radical polymerization are typically found in commercial applications, little has been reported in terms of anionic photoinduced based inks [153]. Nonetheless, the number of research reported on anionic photopolymerization and new photoinitiator systems [154–160] increased over the last decade, most likely indicating a greater interest in this new type of ink considering its promising properties such as low sensitivity towards both oxygen and moisture [45] and the ability to control structure and functionality of the polymer [153]. Oxygen inhibition and shrinkage result in printed parts with decreased mechanical performance and geometrical accuracy, therefore in the future new type of inks based on other polymerization mechanism such as cationic and/or anionic could be a solution to mitigate this effect.

The polymerization process of photocurable inks can be split into four steps: Photolysis – initiation – propagation – termination [161]. In case of free-radical polymerization, UV radiation is absorbed by the photoinitiator of the ink so that it decomposes into reactive radicals (photolysis). The reactive radicals then approach the carbon double bonds (-C=C-) of the monomer and add to it so that the monomer ends are left with an unpaired electron and became reactive [162] (initiation). Subsequently, monomers bond one after another to the monomers with the active sites enabling the growth of the polymer chain [162] (propagation). Polymerization stops (termination), when the active chain end is inactivated due to three reasons: (1) combination of two growing polymer chains, (2) disproportionation, that is a hydrogen atom of a growing chain transferring to another activated monomer leaving an unpaired electron behind so that the polymer chain rearranges itself to an unsaturated end, and (3) occlusion, which means that free radicals are trapped within the solidified polymer network [163]. In analogy with free-radical polymerization, cationic photoinduced polymerization uses strong acids that are generated from the cationic photoinitiator, such as the photochemically active onium salts [141], to enable the polymerization reaction. In case of epoxide monomers, the photoacid triggers a ring-opening polymerization. In the propagation phase monomers add one by one to the growing cationic polymer chain end [45,141,152]. Termination of ionic photoinduced polymerization is caused by neutralized or stabilized ion [163].

Monomers of different polymerization mechanism can be mixed to one material with both radical and cationic photoinitiators present in order to combine, enhance and fine tuning the properties of the cured polymer [164]. An interpenetrating polymer network will be generated upon irradiation which improves mechanical properties such as Young's modulus, tensile strength, etc. [165,166], enabling functions such as shape memory polymer [167], scaffolds with absorbing and elastic properties for generating dermal substitutes [168] or mechanically reinforcing weak hydrogels for biomedical [169] and food applications [170]. Several combinations such as acrylates (free-radical polymerization) and epoxides (cationic polymerization) were reported [165,171–173]. Kopatz et al. elaborated on the cure kinetics and mechanical properties of a dual-cure resins combining epoxy and acrylate resins [174].

6.2. Curing depth

Very few research studies have investigated the curing depth and photocrosslinking properties of layers printed in material jetting, although a well-controlled curing depth is important in order to avoid for example under-curing which affects the geometrical resolution negatively as semi-cured droplets still spread, resulting in sagged edges

(assuming that no support material borders the build material) [175]. Moreover, curing has a considerably effect on mechanical properties and glass transition temperature as well. Anastasio et al. observed for instance that an increase of curing time and UV-light intensity comes with the increase of the glass-transition temperature and yield stress [176].

Taki et al. and Pierrel et al. measured the degree of crosslinking along the z-direction to quantify the oxygen inhibition [177,178]. Zhao et al. set up a model that predicts the degree of photo-crosslinking/consumption of the vinyl groups of the printed part in MJ, and which has been validated for various print and curing strategies. It was observed that the degree of crosslinking varies depending on the chosen curing strategy and is not homogenous (a gradient has been, for example, detected in the y- and z-direction). This model factored in the photopolymer reaction kinetic, the Gaussian beam light profile and the Beer-Lambert law for describing the light attenuation [179]. Other publications on curing/penetration depth of photopolymer materials exposed to UV-light are based on VPP. Considering that the printed layer height in MJ is in a similar range like in VPP (both in double digits micron range, micro-stereolithography can even do below 10 μm [180, 181]) and that both technologies deploy UV-curable materials, a closer look into the methods and models established for VPP for predicting the penetration depth will be given in the following Section.

Beer assumed that light loses a fraction of its incidence intensity while passing through an optically thin layer [182]. Hence, Eq. 4 was formulated

$$I_s = I_0 * e^{-vs} \tag{4}$$

where I_s is the irradiance of the light after transmitting a path length of s in reference to the incident point $s = 0$ at which the light intensity is I_0 and v the extinction coefficient [182]. Based on Beer-Lambert law, Jacobs defined the intensity for an incident laser beam passing through a resin for stereolithography as shown in Eq. 5,

$$I_s = I_0 * e^{-s/D_p} \tag{5}$$

where D_p (cm) is the penetration depth of the resin. Penetration depth is defined as the depth of the resin for which the irradiance of the laser beam is reduced to $1/e$ (37%) of the incident irradiance I_0 (mW/cm^2) [183] (Eq. 6)

$$E = \int I \ dt \tag{6}$$

The time integral of the light irradiance I is E (mJ/cm^2), named exposure or energy dose [183].

Jacobs proposed a working curve (Eq. 7) for resins printed with stereolithography

$$c_d = D_p * \ln\left(\frac{E_{max}}{E_c}\right) \tag{7}$$

which states the relation between cure depth c_d (cm) of a photopolymer resin upon light exposure, with E_{max} (mJ/cm^2) being the energy of the light at the resin's surface. E_c (mJ/cm^2) is the critical exposure energy dose which marks the pivot point, called "gel point", where the liquid resin turns solid. D_p and E_c can be determined experimentally by measuring the thicknesses of the cured layer c_d for various energy doses E_{max} [183].

Bennet examined several measuring devices for gauging c_d and identified caliper as unsuitable for soft material stylus, while profilometry and confocal laser scanning microscopy yield accurate results for hard specimens [184]. After plotting the obtained values in a semi-log plot, the penetration depth D_p is the slope and E_c the interception of the straight curve with the x-axis [183]. Once the working curve is known, the user can set the radiation setting and increments height (in the case of VPP) according to its desired layer height. Both D_p and E_c

depends on the material formulation and the wavelength of the radiation source [184,185] and therefore must be determined each time a new material or light configuration is deployed. A dependence of D_p and E_c on light intensity had been observed, but is considered negligible [184].

Since Jacob's proposed working curve in 1992, several research studies suggested further improvements and modifications of this model. Uzcategui et al., for instance, improved the Jacob's working curve by factoring in the effect of oxygen inhibition on the polymerization kinetics and introduced a scaling exponent to the working curve [186]. Several works addressed the effect of particles and modified the working curve accordingly to better predict the cure depth taking scattering, absorption and particle size into consideration [187–190]. Champion et al. recently proposed another more efficient way to predict the Jacob's parameter D_p and E_c. Instead of printing and measuring several specimens, they suggested to calculate D_p based on the molar absorption coefficient of the resin ε_λ and the photoinitiator concentration $[PI]$ according to the equation of Bouguer-Lambert-Beer (Eq. 8):

$$D_p = \frac{\log(0.37)}{-\varepsilon_\lambda * [PI]} \tag{8}$$

The molar absorption coefficient is calculated based on the absorbance measured on a UV-Vis spectrophotometer. E_c is determined by the exposure time and irradiance required at a RT-FTIR or photo-DSC to reach a certain gel point. The point at which the gel point occurs can be quantified by the Stockmayer equation (Eq. 9)

$$a = \frac{1}{f - 1} \tag{9}$$

with a being the critical value leading to the gel point and f the functionality of the branch unit [191].

Other approaches to determine the curing depth could be by measuring the degree of photocrosslinking of an UV-curable ink at several height perpendicular to the plane of printed layer. Commonly used devices of determining the degree of conversion of a UV-curable material are fourier transform infrared spectroscopy (FTIR) [192], confocal Raman microscope [193] or photo differential scanning calorimetry (photo-DSC) [194].

6.3. Curing process

6.3.1. UV-sources

A proper, stable and efficient curing process depends on an optimum match of the UV-lamp's emitting spectral range, irradiance and time of exposure, radiation in the infrared spectrum (for surface temperature) and the optical and physical properties of the UV-curable material [37]. UV curable inks are commonly cured under a mercury vapor arc lamp. Mercury arc lamps generate photons by electrical discharge in the mercury vapor resulting in a transition between the excited levels [47]. Mercury arc lamps doped with metallic halides enable emission spectrum from around 200 nm up to the UV–visible range of 450 nm [37,47, 195]. The broad range is required to achieve both surface-cure [37] (UV-C: 200–280 nm, UV-B: 280–315 nm) and through-cure (UV-A: 315–380 nm) of a cured film [196]. Short UV-C wavelengths are primarily absorbed in the surface while longer wavelength penetrates deeper into the material [37]. Moreover, photoinitiators will absorb the radiation of the wavelength to which they are sensitive to and prevent light from reaching molecules in the deeper area. UV-curable inks therefore normally contain more than one photoinitiator, requiring curing at more than two wavelength ranges to enable proper curing across the depth of a layer. Applying short UV-radiation only causes low adhesion to a substrate, insufficient mechanical and chemical resistance while curing with only a long UV-wavelength range results in tacky surface and poor crosslinking, hence a lack of scratch and abrasion resistance [34,37,196]. Curing of thick layer film (> 50 μm) requires

long wavelength [37,196]. Thick pigmented layer can be, however, better cured by electron-beam technology [161].

UV-LED lamps are becoming more powerful due to its rapid pace of development and therefore suitable for industrial application. UV-LED lamps are a monochromatic radiation source and is primarily available at wavelengths 365 nm, 385 nm, 395 nm and 405 nm [196], although the wavelength 395 nm is most commonly used as it is up to date less expensive than other UV-LED lamps [34]. UV-LED are more stable and can also be instantly turned on and off without any warm-up phase which saves time and capital as well [195]. Since UV-LED lamps emit a very narrow wavelength range in contrast to mercury arc lamps, they are considered more energy efficient, as mercury arc lamp's broad spectrum contains wavelengths to which the photoinitiator is not sensitive to, hence consuming energy which is either not used or turned into heat that can have a detrimental effect on heat-sensitive substrates. One drawback of UV-LED is that it is still an emerging technology, offering only powerful sources in the UV- A section up to date, though much work is currently underway. Another issue is associated with the material. As mentioned above, the wavelength determines the penetration depth of the incident light, that is why UV-curables are often optimized for a broader wavelength range. Adapting the formulation of an existing ink to a monochromatic UV-LED-lamps implies a change of final physical properties, which poses a challenge to the industry [197]. To cure a UV-curable ink that is optimized for treatment with a mercury UV-lamps, Taki and Sawa utilized a hybrid UV-LED, that is, a LED-lamp containing three different wavelengths, to achieve comparably curing results [197]. UV-LED also offers in terms of safety issue a good alternative to mercury arc lamps as mercury has long been identified as toxic and poses a risk to both workplace and environment [198].

### 6.3.2. Curing strategies

In general, commercial MJ printers include the steps (1) printing, (2) levelling and (3) curing, whereby the curing takes place after the levelling and after the completion of one layer. Cheng et al. deploys a printing strategy similar to the one used in commercial MJ printers [199]. Zhao et al. and Elkaseer et al. on the contrary do not include a flattening device in the printing process, thus the printed layer was cured immediately upon deposition [179,200]. Tilford et al. reported to apply an additional "pinning" step each swathe before the levelling step which is followed by a curing step [5].

In the graphical industry "pinning" is commonly found in printing labels and packaging or marking and is a well-established method to control the print resolution [201]. Pinning describes a slight curing of a deposited droplet right upon its deposition while it is in the process of taking on its shape on the substrate. The pinning takes place with a

fraction of the radiation energy level required for full cure, so that the droplets are turned into a gel-like state. At this state, the adhesion to other printed droplets is still possible while further spreading of the deposited droplet is prevented so that a precise pattern is possible [179]. Pinning is not only important for the graphical industry but also for MJ technology. Zhou et al. examined the merging process of several adjacent droplets and suggested that the pinning process should be applied between the impingement and the equilibrium state, as the best shape (flat topology) is an intermediate state [202]. Pinning (or curing in general) with an optimum timing and intensity might be able to both increase the printing resolution and enables sharp-edged geometries (Fig. 8).

Although "pinning" is widely applied in the graphical industry, no methods are reported on how to determine the optimum pinning energy or how and when to apply this step within the printing process. Only Caiger stated in his work that 1–5% of the full cure energy dose is to use [38]. Even for VPP, where the gel point is important to know as it defines the critical energy, there are no agreement on how the gel point is defined. Depending on the approach one choses, the gel point for acrylate resins ranges from 5% to 35% of the full cure energy [191]. Hence, further research works are required to clearly define the degree of curing in the pinning step. Moreover, subsequent process steps, such as flattening (if deployed) might limit the degree of pinning as well, as the state of the material defines whether it adheres to the flattening device or not. It may also be worth investigating, if pinning is actually required. These days, UV-LED lamps are deployed for the pinning process as UV-LED performs more efficiently compared to conventional UV-light sources [201].

3D printed parts printed out of UV-curables normally still contains a certain amount of non-cured resin without any post-cure treatment. It is reported that post-curing improves the crosslinking density and therefore the overall mechanical properties, surface hardness and thermal stability of a printed part [186,203–206]. However, high dose of energy can increase the brittleness and a drop in percent elongation at break as well [205]. Post-cure processes that are mentioned in the literature are curing in an UV-chamber, thermally, deploying both approaches, in a passive process without any additional radiation or by means of an electron beam [186,203,205,207,208]. In case of radiation post-curing, the resulting properties depend on the wavelength, the temperature and the post-cure time [203,207,209]. Heat can also further drive the polymerization to a certain degree, leading to additional cross-linking of trapped and unreacted monomer within the resin. The higher the temperature, the faster the cured section is reaching a fully cured state. Increasing the post-curing temperature can increase the overall achievable mechanical properties as well, but the temperature ought to
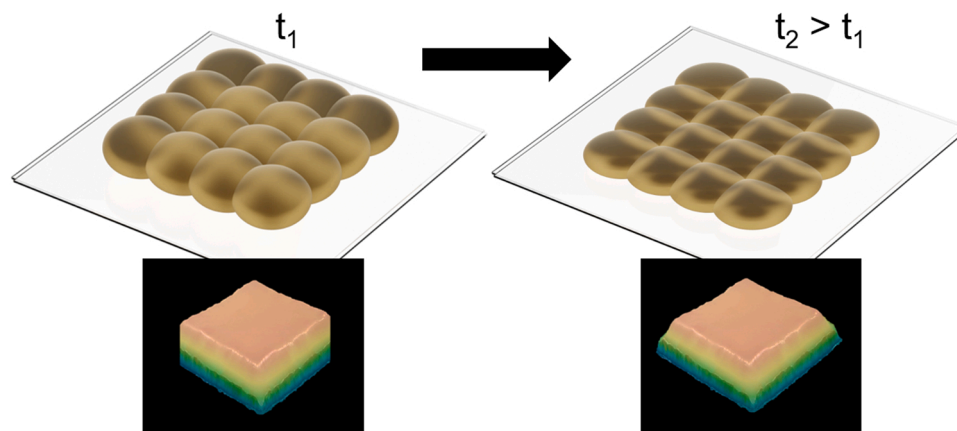
Fig. 8. The effect of pinning on a layer generated by material jetting. Accuracy of a printed layer and resolution can change due to further flowing of the droplets over time (t), when not properly cured. Droplets can be prevented from further spreading by applying slight curing (pinning), however the timing and the intensity of this curing step matters.

be kept below the heat deflection temperature [209]. Asmussen et al. reported a strategy to dope UV-curable resin with silver nanoparticles to induce further heat during the post-curing process as the UV-radiation is absorbed by silver nanoparticles as well [210]. Some photosensitive resin contains heat-sensitive photoinitiators as well, so that full conversion is reached by a thermal post-cure [186]. Uzcategui et al. observed in their study that the dual-cure resin reaches the maximum mechanical properties regardless of the level of conversion after photo-radiation [186]. While the majority of the literature deals with the post-cure effect for VPP, only one study to our knowledge examined post-curing on a inkjet-printed part, which observed that post-curing is able to homogenize the gradient of the level of conversion of a printed specimen [206]. Unwanted effects of post-curing can be additional warping and yellowing of the printed part [208]. A critical investigation into the time and the degree of post-curing for material jetting should be carried out as well. Both under- and over-curing have a detrimental effect on the mechanical and thermal properties. Over-curing may cause internal stress due to shrinkage or even breakages. Poorly cured layers may lead to migration of unreacted materials, low mechanical properties und geometrical inaccuracy.

Additionally, it is suggested to examine which curing strategy (with or without pinning, which wavelength, which UV-source, curing between each swathe, between each layer or every n-layers, with or without post-curing) can achieve best high accuracy printing with high mechanical performance. Zhao et al. proposed a model which predicts the level of polymerization of a printed part taking into consideration the relevant UV-radiation parameters and printing strategy [179]. Producing multi-material components within a single process includes a high chance that the materials being combined need different curing conditions of the respective curing methods, which in turn bring in challenges of their own. In this case perhaps selective curing of multi-material inkjet-based 3D printing by means of laser could be a suitable approach. Furthermore, curing strategies for printing 3D multi-material parts with heterogenous curing conditions, such as UV-curable droplets deposited next to a solvent-based nanoparticle silver ink are to be examined as well.

7. Quality issues in material jetting

In the following Section commonly occurring quality issues in material jetting, such as shrinkage, inconsistent layer height, oxygen inhibition, and coffee-ring effect, the latter one a common issue of particle-loaded inks, are presented and possible solutions are reviewed.

7.1. Shrinkage

An important factor in the curing process of inks is its effect on the resultant dimensions of the printed part. Shrinkage, which in some cases results in warpage, of UV-cured layers poses a huge problem when it comes to printing thin delicate structure or generating UV-curable layers on thin substrates. Yang et al. examined the dimensional accuracy of printed features using a ProJet 3D printer, which uses wax as support material. Printed features in the millimetre range resulted in a small amount of shrinkage. Furthermore, the dimension of the whole printed parts was also observed and found to be smaller than designed. To compare these results to another support material, the same part was printed using PolyJet technology, which did not achieve these resolutions, due to a fusing of support and build material and thus resulting residue [97]. Kechagias et al. investigated the dimensional accuracies by parts produced by PolyJet technology in regard to the parameters layer thickness, use of support material and the size of the model itself in regards of external dimensions. They concluded the size of the model as well as the use of support material as influencing parameters in the x-direction, while layer thickness influenced precision in both the x- and y-direction. The model size was examined to be the dominant factor for precision in the z-direction. Both shrinkage and enlargement of parts

was observed [99]. Yap et al. also investigated layer thickness and the surface type finish, but also looked at the location of the part on the build plate. Contrary to the study by Kechagias et al., the use of support material to preserve geometries was observed to be most influential along the x-axis, while location on the build plate was for the z-axis. These differences were attributed to support material keeping the part in shape and avoiding deformations, as well as different UV-intensities on different build plate areas. Furthermore, features along the z-axis were found to be most accurate to theoretical values [100]. Further examination on how to mitigate the shrinkage issue without using support material, in order to reduce waste material, such as by proper curing strategy, or deploying inks based on different curing mechanism should be conducted in the future.

7.2. Layer height consistency

Consistency in the layer height and surface evenness is a crucial aspect in printing 3D parts in a reliable way. Zhou and Loney simulated the interaction of multiple droplets so that based on these findings droplet deposition can be controlled and predicted for the application in manufacturing and for improving the printing outcome omitting the use of e.g., a flattening device [202]. However, these results were generated upon ideal conditions, which means assuming droplets with consistent shape and size and accurate distances between two droplets. In reality, the quality of a 3D printed part can be subject to droplets variations in drop volume, drop shape, deviation in the travel trajectory resulting in positioning inaccuracy, substrate irregularities [211], nozzle failure due to nozzle clogging [212] or shrinkage upon curing [200,213,214] (Fig. 9). Slightly deviating droplet properties might only result in minor and negligible irregularities in one layer, but add up to major defects in 3D printed parts as several hundreds or thousands of layers are printed.

Particle suspensions are especially susceptible to nozzle clogging. The presence of solid particles can cause the ink to clog at the nozzle, leaving it unusable, as ink is unable to pass through the nozzle. To maintain printability, different measures can be taken. Lee at al. investigated nozzle clogging for inks containing ZnO particles in varying amounts and in combinations with a surfactant. The overall range of printable ink compositions examined was for Z numbers between 2.5 and 26. However, this range is not sufficient to characterize the printability of the investigated ink composites. Furthermore, inks containing particles the size of 1 μm or larger caused the nozzle to clog presumably due to flow-induced aggregation, even if the inks were in the aforementioned range. This was shown via the pressure increase of the inks, where larger particles resulted in a sharp increase in pressure unlike smaller particles. It is theorized, that the pressure increase occurs due to particles accumulating in micrometre-sized impurities inside the nozzle. For particles smaller than 1 μm, it was concluded that concentration should not exceed 500 ppm and the total number should be below 7 $\bullet 10^5$ particles per mL to ensure printability. A similar accumulation can also occur through drying and evaporation around the nozzle, leaving behind solid material that can block the nozzles [3].

One way to combat the irregularities caused by the substrate is by printing few layers of support materials first which are then flattened, so that a fully covered homogenous base layer of support material serves as a substrate for next layers of build materials. Excessive materials above the target layer height can be removed with a levelling device as well [199]. Variations of droplet size and shape, and issues such as positioning error or missing droplets during a print job are by contrast more difficult to compensate. Several works were conducted in exploring various concepts of feedback control algorithm for compensating the error of these issues in inkjet-based 3D printing [211,214–216] or in other photopolymer-based printing technology [213]. Huang et al. used a deep-learning method to study videos capturing the flow pattern of a droplet which can be used for the prediction of the jetting behavior [217]. Segura et al. built an analytical framework to detect abnormal droplet jetting behaviors from videos [218].
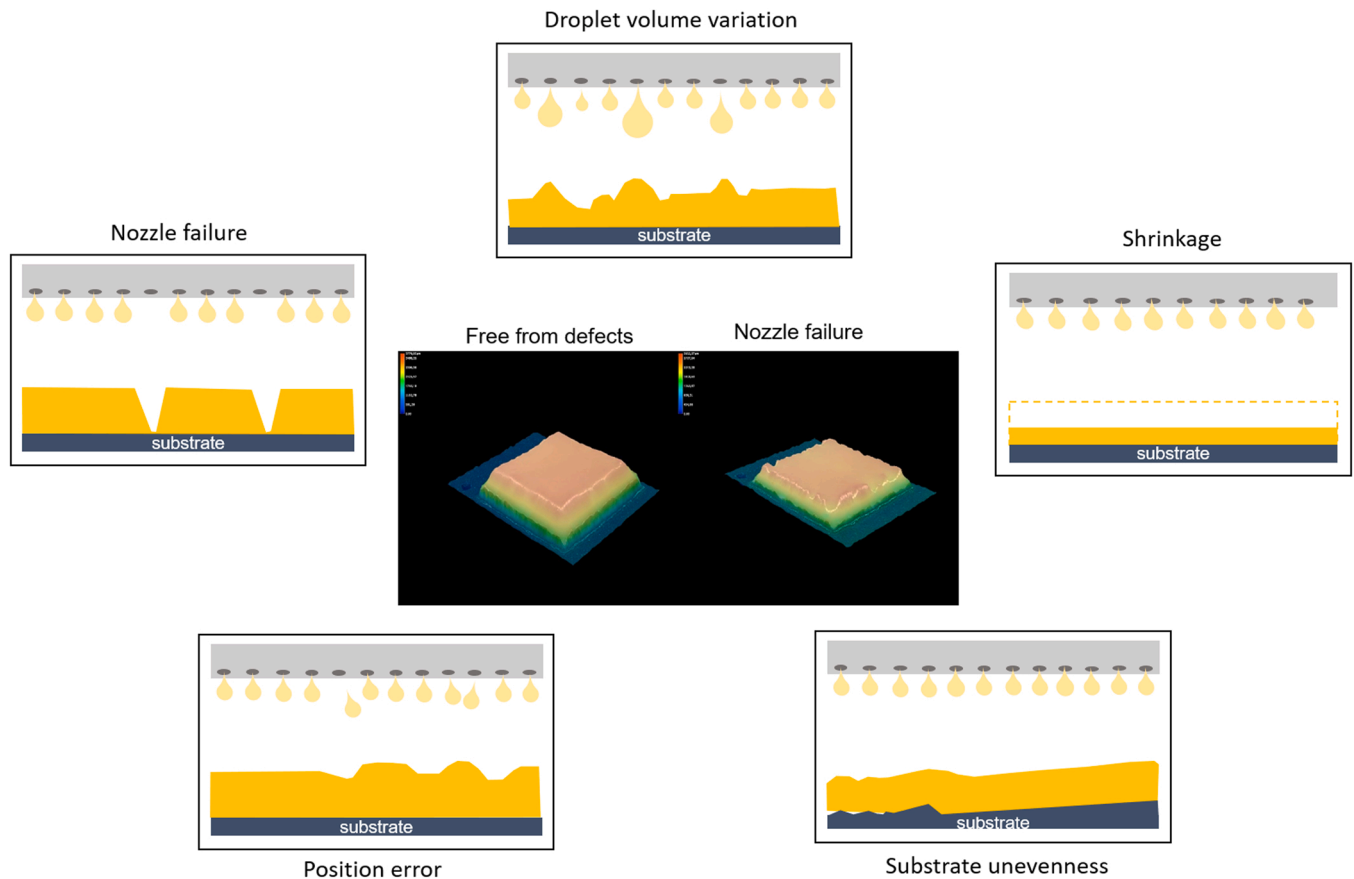
Fig. 9. Various defect scenarios of a 3D part generated with material jetting based on UV-curables.

The levelling device has essentially two functions: First, it serves as a planarizer, which smooths the surface of the printed layer, as the topology of the printed arrays of droplets appears slightly wavy even after merging. The second function is concealing irregularities of the surface caused by malfunctioning nozzles (i.e. skew jetting trajectory, variable nozzle volume) by taking off protruding material that exceeds the target layer height. Thus, a layer levelling device enables reproducible and consistent printing quality. The levelling device is in most cases a roller to which a blade is attached. The blade takes off the UV-curable material from the roller surface and directs it to a waste container [13,219–224]. One drawback of using a roller is, however, the waste material caused during the flattening process. Some alternative approaches to reduce or even omit the need for a roller are for example the implementation of data correction filter to adjust individual nozzles [225] or optimizing the deposition parameters based on a droplet shape evolution model [202]. There are no systematic investigations and clear understanding on how a roller interacts with a printed layer, yet. Except for a study by Cheng et al. [199], exploring the effect of roller direction, roller rotational speed and surface roughness of the flattened layer, and a plot in a patent by Mimaki [222] showing the interdependence of film thickness of drawn ink and the peripheral speed of the roller, not much can be found in the literature. Generating smooth layers with a consistent thickness is a challenging issue that still needs addressing, and it is important to study the interrelation of process inaccuracy and final part geometry.

7.3. Oxygen inhibition

Acrylate-based inks or rather free-radical polymerization are subject to oxygen inhibition which carries out the inhibition by essentially consuming the radicals generated upon irradiation or by terminating the cross-linking process due to: (a) quenching of the excited state of the photoinitiators upon radiation (b) reaction with the radicals produced from activated photoinitiators (c) reaction with radicals of the growing polymer chain. These competing reactions generate peroxide radicals which are more stable and less reactive und therefore do not contribute to polymerization [226–229]. Consequently, oxygen inhibition leads to lower reaction rates and diminishes the degree of conversion and resulting in tacky surface with poor scratch resistance and matt surface as oxygen inhibition is more pronounced near the surface [227,230]. Nanoindentation is one way to characterize the hardness of the surface [206]. Oxygen inhibition can also cause quality issues such as storage stability or discoloration [231]. The rate at which oxygen molecules interact with the reactive species is faster than the propagation rate, hence the polymerization is delayed until all oxygen molecules are consumed [228]. Besides, the diffusion rate of oxygen into the deposited material must be lower than the generation of radicals to start the polymerization process [229]. Several works on modelling the free-radical polymerization process taking the oxygen inhibition into account were carried out [229,232–237].

Abundant ways to minimize or overcome the inhibition effect exist such as by curing in an oxygen-free atmosphere, for instance in nitrogen [227,238], argon [229] or carbon dioxide [230], prepurging specimens with low layer thickness ($<10\ \mu m$) with inert gas before curing [231] or by using films as barriers [173,231,239], although the latter way would not work for 3D printing. Other solutions are deploying oxygen scavengers and other additives to suppress, reduce or desensitize the system to oxygen inhibition [231,240–242], curing with higher intensity light, dose or including more reactive monomers or higher amount of photoinitiator in the ink formulation, so that a great amount of photoinitiators are generated in a shorter period of time to overcome the diffused oxygen [38,47,150,231,238,240].

The thickness of the oxygen-inhibited layer is reported to increase

with lower radiation intensity [234,243]. However, higher intensity will reduce the curing depth [232] and therefore affecting the mechanical properties while a high photoinitiator level increases the formulation cost [38,238]. Other mitigation approaches are printing larger droplets to decrease the surface to volume ratio and therefore decreasing the amount of diffused oxygen, using water-based UV-sensitive ink (water allows higher molecular weight and therefore more reactive species due to its low viscosity [38,238]), curing with electron beam as described above (photoinitiator-free formulation), deploying UV-C radiation for avoiding tacky surface [244], dual-wavelength polymerization [245, 246] or deploying ink based on cationic polymerization that is inherently free of oxygen inhibition [150]. Although cationic polymerization can be inhibited by humidity instead [142], Atsushi et al. observed that the inhibitory effect caused by oxygen on free-radical polymerization is greater than humidity on cationic polymerization [150]. Further details and reported studies on oxygen inhibition were reviewed by Ligon et al. as well [231].

Nevertheless, it is worth emphasizing that very limited works attempted to address the oxidation effect on 3D parts printed with MJ or droplets [150,226], while the large body of the aforementioned works investigated this effect either for coatings generated with a coating rod, by spin-coating or by molding, and with thickness ranging from few micrometers to few millimeters [173,177,178,226,227,233,234,239, 247]. However, as the layer height in MJ is normally around 10 μm, it is very likely that the conclusions derived in these studies are applicable to inkjet printing. Although the oxygen solubility decreases with increasing temperature (the printing temperature of UV-inks is often around 50–60 °C), the lowered viscosity of the ink enhances the diffusion of oxygen. The enhancement of the diffusion rate by elevated temperature had been observed by Studer et al. to be a more dominant factor in the polymerization process of an acrylic resin [248]. Despite the findings of Studer et al. [230,248], no other works on oxygen inhibition investigated the effect of viscosity.

Both characteristics of inkjet-printing, thin layer (normally not more than double-digits layer height) and a small droplet volume make it more susceptible to oxygen inhibition [150,226,248]. Moreover, inkjet inks have inherently lower viscosity of normally 5 mPa•s to 100 mPa•s in order to fit into the requirements of industrial piezo-inkjet printhead compared to a photopolymer resin used for photopolymer vat technologies starting from 100 mPa•s, which indicates that atmospheric oxygen diffuses more easily into an inkjet ink, favoring oxygen inhibition [38, 150,238]. Results derived from studies performed with a photopolymer vat technology [236,249] can only be transferred to a limited extent to material jetting, because the printing takes place in a vat filled with resin containing different amount of oxygen. For a deep understanding of how and to what extent oxygen inhibition plays a role in the three-dimensional inkjet-based printing process, further studies are required to have a closer look at this issue.

The influence of oxygen on degree of conversion can be determined by means of confocal laser Raman microscopy [177,178], photo-DSC [226,227] or FTIR spectroscopy [177,239]. Taki et al. and Pierrel et al. measured with Raman microscopy along the depth of a multi-layered film [177,178]. Taki et al. set up a numerical model simulating the conversion behavior and explored the effects of the UV-radiation intensity, irradiation time, photoinitiator concentration and concentration of dissolved oxygen on the oxygen concentration and conversion distribution for a bilayer model [178]. Pierrel et al. investigated the effect of oxygen-dissolved region on mechanical property experimentally [177]. Both observed that the top region of each newly printed and cured layer is exposed to oxygen from the environment and therefore first poorly cured. However, a subsequent layer photopolymerized on top of it will then homogenize the level of conversion to a certain degree as the initially unreacted monomer of the previous layer reacts upon radiation of the subsequent layer as well (Fig. 10) [177, 178]. These results suggest that the conversion distribution in an inkjet-printed 3D structure is nearly homogenous.

Oxygen inhibition can contribute positively to the interfacial mechanical properties of a 3D printed part as reported in Zhao et al. [239]. Oxygen dissolved in the surface of each layer retards the conversion rate at the surface, offering a better adhesion to the subsequent layer and therefore improving the interfacial strength of a layer-wise built part. Pierrel et al. observed that the mechanical properties improve in comparison to a single layer by applying a second layer of photopolymer despite the presence of oxygen inhibited layers at the interface [177]. Additional work is still required for investigating the effect of oxygen inhibition on parts printed with material jetting with regards to its effect on mechanical properties, delamination issues, migration of photoinitiators in less cured interlayer. Approaches ought to be determined how to mitigate the effect of oxygen inhibition.

7.4. Gas dissolvement

An important factor that should be considered is the level of oxygen present in inks as, firstly, oxygen is linked to the decomposition process
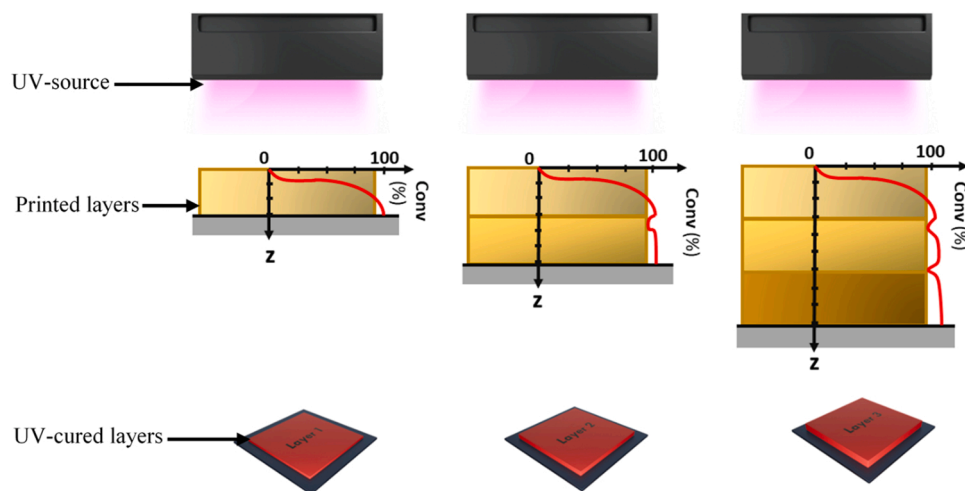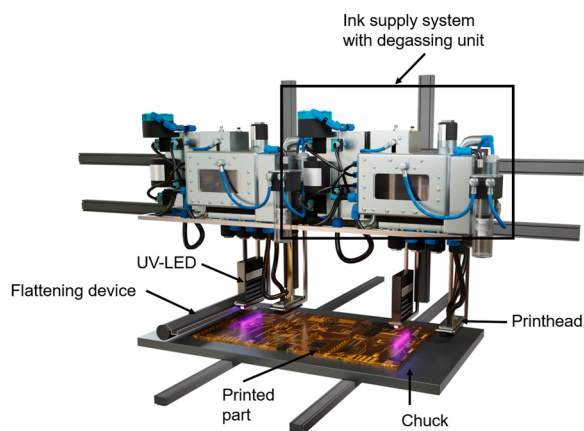

Fig. 10. Oxygen inhibition and its effect on material jetting parts. Each newly printed layer is subject to oxygen inhibition in the upper regime. This less-cured surface will, however, be further cured, if a subsequent layer is applied and cured so that the whole part shows an almost homogenous conversion rate with a slight dip at the height of the interface between layers.
Adapted from the illustrations by Taki et al. [178] and Pierrel et al. [177].

of organic material, because peroxides and other chemical groups are formed that cause degrading [101]. While different colored inks degraded differently, because of their different chemical composition, Blaznik et al. observed that oxygen contributes most to the photo-degrading process of commercial aqueous inkjet inks of all colors tested [103]. Secondly, oxygen also affects the curing of UV-curable inks, as mentioned in the previous Section. The use of an inert gas like nitrous or carbon dioxide can be utilized inside the ink system to keep oxygen levels to a minimum [54]. Thirdly, the printing process can also be destabilized and blocked by air bubbles caused by dissolved gas in the ink due to a phenomenon called rectified diffusion. Rectified diffusion describes the growth of a bubble upon oscillations in acoustic fields caused by the reverse flow of gas from the liquid into the bubble [250, 251]. For this reason, some inks require additional membrane degassing units within their ink supply system (Fig. 11). Membrane degassing extracts dissolved gas from a liquid by applying a vacuum while the liquid passes the membrane. For suspension inks it is reported, that flow rate influences clogging of the nozzle, with higher flow rates leading to less clogging, presumably, because higher flow rates tend to break up aggregates before they are large enough to cause clogging [2].

7.5. Coffee-ring effect

The coffee-ring effect is a phenomenon that occurs in particle-loaded solvent-based inks. It describes the deposition of particles at the outer edge of the original ink droplet, that occurs during evaporation. This is caused by a higher rate of evaporation at the outer rim of the droplet [90]. On the edge of the droplet, where three different phases are in contact, evaporated ink causes liquid ink from inside the droplet to move to the outer edge. The resulting capillary flow transports particles to the outer edge. Multiple approaches of mitigating the coffee-ring effect exist [252]. Decreasing the capillary flow, that causes the movement inside the droplet, is one of them [253]. This can be done by slowing down the evaporation process. Experiments using a cooled substrate demonstrated a reduced coffee-ring effect. Increased humidity levels were also shown to reduce this effect as a higher humidity reduces the evaporation rate. Droplet size also seems to have an effect. This is explained by the difference between solvent evaporation time and solute movement time. As droplet size increases, the solute needs increasingly more time to move inside the droplet, while the rate of evaporation at the edges does not get effected by droplet size. Experiments showed, that a decrease in droplet size reduces the coffee-ring effect. Similar effects can be achieved by inducing and increasing a Marangoni flow inside the droplet. The Marangoni flow occurs due to high surface tension liquids extorting

a stronger force on surrounding liquids, then lower surface tension liquids. This can be achieved by adding a high boiling point low surface tension liquid to the ink. Similar results can also be achieved by adding surfactants to the ink. However, the coffee-ring effect can be utilized when printing with solvent-based inks. The rings formed by evaporating droplets have been used to create conductive patterns by using carbon-nanotubes as solutes. Furthermore, by combining coalescing droplets with the coffee-stain effect, two parallel lines were created, as droplets merged into a single line and the capillary flow moved the solutes to the outer edges [85].

8. Current and potential applications

In this following Section a summarized overview of advanced applications of material jetting and functional inks is listed.

8.1. Printed electronics

A large part of reported applications of functional inkjet inks are printed electronics or selective coatings, but for pharmaceutical and biomedical applications inkjet printing serves as a promising technology, too. Nonetheless, it should be noted that these inks are predominantly applied rather in a 2D manner than 3D. Nevertheless, reviewing these examples can help exploring further potential advanced applications for material jetting. Ko et al. and Sowada et al. demonstrated clearly by generating 3D pillars and metallic wires from solvent-based nanoparticle-loaded inks [6,254] that once printing of these functional inks are possible, generating 3D structures by material jetting is within reach.

8.1.1. Pressure sensors

Inkjet printing can be used to produce resistive pressure sensors by printing conductive silver nanoparticle (AgNP) layer directly onto a polydimethylsiloxane substrate and encapsulated by a VHB tape. The pressure is obtained by measuring the change in electrical resistance caused by pressure-induced strain in the printed AgNP thin film. A sensitivity of up to $0.48\ kPa^{-1}$ was studied and achieved by Lo et al. [255]. Griffith et al. reported a highly sensitive pressure detector prepared by inkjet printing of electroactive organic semiconducting materials and the detector was able to convert shock wave inputs rapidly and reproducibly into an inherently amplified electronic output signal [256]. Jeong et al. manufactured an electromagnetic pressure sensor by printing conductive patterns on a flexible film [257].

8.1.2. Transistors

CNT-based thin-film transistor can be printed on a Kapton substrate. The very small channels can be formed by employing the chemical force between inks. Grubb et al. has achieved the transistor with operation speed up to 18.21 GHz [258]. Sing et al. printed electrodes of the organic thin film transistors with inkjet printing [259]. Park et al. fabricated thin film transistors from single-walled carbon nanotube with inkjet printing. [260]. Mangoma et al. printed organic electrochemical transistor (OECT) for the use as a neuromorphic device, where the electrodes and dielectric layers are printed with Fused Filament Fabrication (FFF) and the semiconductor thin film is applied by inkjet printing [261].

8.1.3. Photoacoustic generators

Oser et al. proposed a novel method to produce photoacoustic generators based on inkjet printing with multiwalled carbon nanotubes (MWCNT) and polydimethylsiloxane (PDMS). The printed photoacoustic generators show a good homogeneity and low optical transmission (19 – 21%). The generated ultrasonic pressure (0.39 – 0.54 MPa) and frequency bandwidth (1.5 – 12.7 MHz) can be measured at a distance of ≈ 4 mm with a laser fluence of 12.7 mJ cm^{-2} [262].

Fig. 11. Schematic illustration of a material jetting printer. This multi-material printing system consists of two UV-LED sources and a flattening device for building up a high-quality 3D printed part and two printheads, each of them jetting a different material. The materials are stored and degassed in the corresponding ink supply system.

8.1.4. Capacitor

Zhang et al. presented printable tungsten oxide nanocrystal inks, which allow the assembly of novel electrochromic pseudocapacitive zinc-ion devices. The printed energy storage devices exhibit a relatively high capacity ($\approx$260 C g^{-1} at 1 A g^{-1}) [263]. Bräuniger et al. proposed the one-step printing of liquid carbon precursors to produce high-resolution interdigital micro-supercapacitor (MSC) devices, which have the capacitance up to 151 F cm^{-3} (3.9 mF cm^{-2}) [264].

8.1.5. Solar cells

Besides capacitor, solar cells can be used to provide electricity as well. Pendyala et al. reported an unique approach to fabricating semi-transparent perovskite solar cells with inkjet printing, which can be used in a variety of applications such as tandem cell configuration and building integrated photovoltaics. They demonstrated a new semi-transparent device structure, showing 11.2% efficiency with 24% average transparency without a top metal contact [27]. Schackmar et al. proposed a method to fabricate high-efficiency perovskite solar cells (PSCs) based on all-inkjet-printed absorber and extraction layers, allowing for a scalable and material-efficient deposition. PSCs with a high-quality inkjet-printed triple-cation perovskite absorber layer and a double layer electron-transport layer of phenyl-C61-butyric acid methyl ester and bathocuproine demonstrate an efficiency of $>$ 17% with low hysteresis [265].

8.1.6. Quantum dot light-emitting diodes (QLEDs)

Inkjet printing can be used not only to convert light into electricity but also to generate light. Wei et al. proposed a tailor-made a highly dispersive and stable CsPbX3 quantum dot ink, which can be used to fabricate quantum dot light-emitting diodes (QLEDs). The inkjet-printed green perovskite QLEDs have shown a record peak external quantum efficiency (EQE) of 8.54% and maximum luminance of 43 883.39 cd m^{-2} [266]. Shi et al. demonstrated an in-situ inkjet printing strategy for fabricating perovskite quantum dots patterns by printing perovskite precursor solutions onto a polymeric layer, with a quantum yield up to 80% [267]. Donie et al. presented a method based on inkjet printing to fabricate phase-separated nanostructures (PSNs), which can be achieved with a feature size from a few micrometers down to sub-100 nm and can be used to improve light management in manifold photonic applications [268].

8.1.7. Antennas

Kimionis et al. produced both the substrate, a multi-material foldable structure based on UV-curable inks, and the patch antenna on top of the origami structure based on reactive silver ink, with inkjet printing technology [269]. Rida et al. inkjet-printed flexible antennas on paper-based substrate which can be used as RFID tags [270]. Jilani et al. generated an antenna for 5 G applications on a PET substrate with inkjet printing [271].

8.1.8. Heating elements

Besides generating light, inkjet printing can be used to generate heat as well. Mitra et al. reported the development in the manufacturing of heating elements based on inkjet printing, which are mainly used to influence the temperature distribution and homogeneity. The heating elements were printed with a nanoparticle silver ink followed by thermal sintering on a standard flexible polymer film, which can reach homogeneous average temperature of 100 $^\circ$C over an area of approximately 15 cm^2 at a power supply of 12 V [272].

8.1.9. Thermal insulation thin film

Aerogels have mainly been used as a thermal insulation material for building applications, such as walls and pipes. Silica aerogel ink, which is synthesized by mixing hydrophilic silica aerogel powder, solvent, and other organic additives, can be employed for inkjet printing to produce thermal insulation layers. Koo et al. studied the thermal conductivity of printed silica aerogel thin film and the results show that the thermal conductivity is approximately 0.05 W m^{-1} K^{-1} at 30–300 $^\circ$C, which has potential to be used for thermal insulating applications in micro-scale systems such as batteries and electronic chips [273].

8.1.10. Smart textile

Further studies show that besides rigid substrate, malleable and soft substrates can be used for the printing as well. Therefore, stretchable circuits become crucial for printable electrical devices. The fabrication of stretchable circuits with sinusoidal or horseshoe patterns on poly-dimethylsiloxane (PDMS) can be achieved by inkjet printing of silver nanoparticle ink. Abu-Khalaf's studies have shown that circuit with a horseshoe pattern can undergo an axial stretch up to a strain of 25% with a resistance under 800 Ω [274]. The stretchable circuits allow for development of fully stretchable and wearable sensors. Uzun et al. presented conductive inkjet printable, additive-free aqueous Ti$_3$C$_2$T$_x$ MXene inks for direct printing on various substrates, which can be used to print electrical conduits and microsupercapacitors (MSCs) on textile and paper substrates. They demonstrated the collector-free, textile-based MSCs with areal capacitance values up to 294 mF cm^{-2} (2 mV s^{-1}) in poly(vinyl alcohol)/ sulfuric acid gel electrolyte [121]. Seipel et al. reported to inkjet print an UV-responsive smart textile and UV-LED cured a specifically designed photochromic ink on PET fabric [275]. This smart textile can be used as UV-sensor to detect harmful UV-rays.

8.1.11. Functional membrane

Park et al. demonstrate the synthesis of thin film composite (TFC) flat-sheet membrane for nanofiltration application with inkjet-printed single walled carbon nanotube (SWCNT). The best membrane performance was achieved from the TFC membrane synthesized using 15 cycles of SWCNT printing, where both high water flux (18.24 $\pm$ 0.43 L m^{-2} h^{-1} bar^{-1}) and the high Na$_2$SO$_4$ salt rejection (97.88 $\pm$ 0.33%) rates were demonstrated [276]. The inkjet-printed piezo-electric P(VDF-TrFE) film on silicon was investigated by Banquart et al. and electro-acoustic responses of multi-layer structures, which are specifically designed for high-frequency, single-element ultrasonic transducer applications, were measured in water. The results showed that maximal frequency was centered at 33.2 MHz and had a fine axial resolution at 22 μm, corresponding to a fractional bandwidth at $-$ 6 dB of 100% [277]. This can be used in multi-element transducers for high-frequency imaging applications.

8.1.12. Anticounterfeit

Inkjet printing has shown potential in customized products as well. Mimicking natural melanin structural coloration enables non-iridescent systems with colors that are independent of incidence angles. Kang et al. printed multiple metal nanoparticles of different shapes over each other [278]. Depending on the wavelength of light, different thermoplasmonic images will show up. This printing strategy can be used for anti-counterfeit technology. Shanker et al. have addressed the problem of incidence angles by forming melanin photonic crystal microdomes with inkjet printing [279]. The printed photonic micro-domes with non-iridescent structural coloring might be used for sensing, displays, and anticounterfeit holograms.

8.1.13. Microstructure surface

Inkjet printing can be utilized in preparing templates or masks for photolithography to produce the microstructures. Inkjet printing of a water-soluble polyacrylic acid solution etched the polydimethylsiloxane substrate. The substrate was then cured and rinsed, allowing it to be directly used as a template for creating micro-structured surfaces [280].

8.1.14. 4D-structure

Cui et al. presented a novel 4D printed tunable frequency selective surface (FSS) utilizing a multi-layer mirror-stacked "Miura-ori" structure

that can be applied in numerous mm-Wave, IoT, RFID, WSN, 5 G, and smart city applications. The prototype has a flexible two-layer substrate with conductive traces on both top and bottom. The prototype demonstrates great frequency tunability, angle of incidence (AoI) rejection as well as an operability up to much higher mm-wave frequencies up to at least 28 GHz [281].

8.2. Chemical, biological and pharmaceutical applications

8.2.1. Chemical catalyst

Inkjet printing for heterogeneous catalytic reactions within chemical reactors has been the subject of several investigations. Selective catalytic reduction is a cutting-edge technique for reducing emissions from industrial boilers, gas turbines, and vehicle combustion engines. Costa et al. used the inkjet printing method for the synthesis and deposition of 0.1 wt% Pt/Al2O3 catalyst with a better catalyst morphology, which showed superior activity at lower temperature range compared to the wet-impregnated samples [282]. Willert et al. inkjet-printed a catalyst-coated membrane for electrolyte membrane fuel cells [283]. The use of inkjet printing can be extended to other types of reactions. Inkjet printing can be used to deposit catalystsonto microreactor walls [284]. The microreactor is employed to synthesize organic and pharmaceutical compounds. Therefore, the catalyst requires to be uniformly and precisely immobilized into the microreactor.

8.2.2. Biological constructs and peptide printing

Inkjet printing can be used in cell biology and associated biomedical research, due to its ability to produce high resolution and high precision prints. Inkjet printing is considered one of the most suitable technologies for bottom-up cell deposition for building intricate biological 2D or 3D constructs [285]. Besides, inkjet printing can be used in intracellular delivery and transfection, gene expression modification, single cell sorting, cell microarray, cell micropatterning, tissue engineering, and in vivo cell printing as well [61]. Safaryan et al. proposed a novel method for the controlled deposition of a self-assembled peptides, diphenylalanine (FF), using a commercial inkjet printer, which can be used to produce peptide-based nanostructures for nanotechnological applications, such as nano- and microtubes and microrods [62]. By using this method, the ribbonlike microcrystals based on FF was formed and patterned on different surfaces, showing strong piezoelectric response. These functional properties of FF- based nanostructures can be used in various micro-devices.

8.2.3. Paper chip-based detector

Tetracycline is widely used as a pharmaceutical for treating diseases and as an animal feed ingredient. Inkjet printing paper chip based smart tetracycline detector can replace classical methods for detection of tetracyclines, which relay on huge and expensive setups. The tetracycline detection is realized by paper chip-based enzyme-linked immunosorbent assay [63].

8.3. Material jetting for 3D and 4D applications

More and more material jetting applications based on functional materials are reported in the literature, for instance in the fabrication of microlens [7], PCBs [286], optical prism [287], scaffolds in tissue engineering [288], anatomical models with biomimicking properties [289] and microfluidic devices/ lab-on-chip [290,291]. Adamski and Walczak printed a venturi microflowmeter with material jetting and integrated a MEMS sensor into the flow meter [292]. Walczak et al. created a microvalve with the same technology [26]. Ko et al. fabricated 3D micro metal structure such as pillars, helices or bridges from nanoparticle silver ink with the help of inkjet printing [6]. Sowade et al. inkjet-printed 3D metal pillars of nominal diameter of 120 μm as well which was then encapsulated with an UV-curable ink [254]. Several studies focused on the 3D printing of ceramic pillars by means of inkjet

technology [293,294]. In a recent study, Kriegseis et al. inkjet-printed a 3D ceramic dental implant (abutment) with ceramic inks [295].

Some applications combine either inkjet printing or material jetting with other type of technologies to benefit from the advantages of both manufacturing techniques. Junqueira et al. recently reported a new approach of printed drug loaded tablets by combining FFF and inkjet printing [296]. Roach et al. suggested a similar approach by printing polyimide with inkjet printing on top of a FFF substrate [297]. Anelli et al. printed a solid oxide fuel cells by deploying robocasting and inkjet printing [298]. Picha et al. combined material jetting and direct deposition of polymer fiber mats in order to create fiber-reinforced soft composites [299]. Stäbler et al. printed conductive tracks with inkjet printing on fiber-reinforced FFF printed substrate to demonstrate its potential for the fabrication of low cost satellites [300]. Because of the poor surface roughness of FFF printed substrates, Stäbler et al. printed a dielectric ink onto the substrate prior to printing the conductive ink.

Moreover, due to the easy implementation of multiple printheads in MJ, some view this technology as the key enabler of multi-material additive manufacturing. Different ways of how multi-material printing are so far realized in inkjet printing. One is printing functionally graded materials by depositing two materials in the manner of a composite material, so that the property of the resulting material can be tuned by the ratio of the base materials [301–304]. Aghaei et al. created components with functionally graded properties ranging from soft to hard structures [10]. Another way is the printing of highly sophisticated multi-color models [305,306]. The third application is printing multi-material object in the manner that the part consists of individual areas based on one material [307,308]. Moore and Williams demonstrated the printing of a multi-material 4D part with elastomer active hinges [12]. It must be mentioned that most above referenced research works have been conducted on a PolyJet printer. Raza et al. introduced a multi-material printer which can print metal, elastomer and UV-curables [309]. Tilford et al. developed a fabrication system containing an inkjet printing module which prints microelectronics from conductive, insulating and support material [5].

9. Gaps and future prospects

Looking at the aforementioned review it is not so difficult to see that while material jetting has tremendous possibilities for manufacturing industries, a number of research and technological developments identified above are required to advance the state-of-the-art and enable material jetting to be used much more widely and in a number of new advanced applications. In this Section, the gaps and future prospects are subdivided for the sake of readability, but it must be emphasized that all process steps are linked together meaning that any changes might have serious consequences for another process step. Therefore, a full knowledge on the effect of printing and curing parameters and conditions, such as drop volume, drop distance or the use of inert gases, on the properties of the printed component is essential and is still to be acquired, if the process is to be extended to large-scale manufacturing.

9.1. UV-curable inks in MJ

Today UV-curable inks for MJ are still limited in their mechanical and thermal properties due to the use of low-molecular weighted polymers to ensure low viscosity. Moreover, the curing mechanism of currently commercially UV-curable inks is mainly based on free-radical polymerization, causing several inherent problems, that is (i) the curing of the surface layer may be disrupted by the presence of atmospheric oxygen leaving the surface sticky and (ii) interlayer regions are less cured and increase the risk of migration of toxic photoinitiators and monomers and (iii) less cured interlayer regions might be the source of delamination and (iv) volume shrinkage due to polymerization process will affect the geometrical accuracy. The development of inks with alternative polymerization processes as described above in combination

with higher polymer load for better mechanical properties, additional ink treatment (degassing) or suitable printing environment (inert gas) would be important to mitigate the issues mentioned above and for extending the range of applications of jettable inks. The development of new inks with multiple functionalities is a priority to extend the range of advanced applications of material jetting.

It has been noted that highly viscous inks are recommended to improve the mechanical strength of MJ components, but present a challenge in terms of printing. Recently, printheads that are able to jet higher-viscous inks emerged but the comprehensive understanding of jetting behavior necessary to fully exploit the capabilities of these devices has not yet been developed. With the emergence of new functional inks that contain higher polymer load or particles, understanding and controlling viscoelastic fluid behavior of the ink is paramount to deploy MJ as an industrial manufacturing technology. Not only does viscoelastic inks behave differently to Newtonian fluids in terms of droplet formation, but they will most likely affect the subsequent steps of MJ such as drop impact, drop merging, therefore layer formation and layer levelling step (if applied). Hence, it is highly recommended to examine the effect of viscoelastic fluids on these mentioned process steps.

To date, there is no practically applicable method to determine the optimal jetting parameters – especially the waveform – of an inkjet process based on the characteristics of the printhead and the ink. Such a method is required in order to accelerate the development of new inks with desirable properties and the corresponding optimal and stable jetting parameters. Of course, other properties of the inks that contribute to jet stability need to be considered. These will include: effects of gas bubbles dissolved in the ink, ink recirculation flow conditions, meniscus pressure. In addition, the long-term effects of heating UV-curable ink at the printhead on, for example gas bubble formation, chemical and curing behavior require investigation.

9.2. Drops generation and layer formation

It is important to obtain the best possible control of the ink droplets for optimum resolution, in particular precision control of droplet size and droplet spread on the substrate/previous printed layer. One promising approach is to selectively modify the surface by means of plasma treatment to control the droplet spreading. The functionalization of the surface by plasma treatment depends on various process parameters and diminishes over time, hence a systematic investigation of these topics is suggested.

Obtaining a consistently accurate layer thickness remains a challenge as well. A layer levelling step applied before curing is a common step which can be found in current commercial MJ systems. The layer flattening step aims at smoothing the surface and ensures the consistent target height. However, so far there is still a lack of understanding on the mechanism involved in this flattening step as very few research works have been conducted in this matter. It should not be forgotten that the flattening step generates considerably amount of waste material which could be reduced by replacing this subtractive step by an in-loop control of printed layer height. Some works have been reported in this matter, but further improvement of these approaches in terms of higher efficiency are recommended.

The direct production of end-use products by material jetting is an increasing trend that requires greater precision in the process and improved material performance, with enhanced toughness in the final product. During the manufacturing process it should be possible to control the size and shape of the ink droplets and the topography and consistency of the surface formed on the substrate. In the post-process phase it should be possible to measure the geometry and dimensions of the manufactured component and to detect the presence of faults, both surface and internal. In order to achieve these goals, research and development must determine any correlation between droplet formation and deposition, layer generation and functionality of the manufactured component. Another key area of research is to enhance the geometrical

accuracy of planes orthogonal to the x-y-plane without the use of support material. Possible approaches could be selective modification of surface energy (e.g. by plasma treatment) to create small drop sizes and to control the droplet spreading, achieving high precision deposition at the border of a printed pattern.

9.3. Curing process

No practical methodology has been proposed so far on determining optimum curing conditions and proper curing depth for generating 3D parts based on material jetting, even though curing parameters have a considerably impact on the resulting 3D part in terms of mechanical and thermal properties, migration of hazardous components of the UV-curable ink and geometrical accuracy. Methods explored for VPP might be applicable for MJ, but is subject to investigation. Conventional methods on determining the degree of conversion, such as FTIR or Raman microscope could also be used for gauging the cure depth by measuring along the depth (z-axis). However, due to the low penetration depth of these methods of around 1 μm, slicing along a printed layer might to be necessary in order to measure along the thickness of a printed layer, although this approach would be deemed impractical. Another model predicting the degree of photocrosslinking for MJ takes into consideration the kinetics of photopolymerization and the illumination conditions has been reviewed. This approach should be further explored as well.

Another matter which should be subject to further investigation is the optimum curing strategies for high-precision and high-speed production of material jetting. So far several curing approaches are reported in the literature: commercial material jetting printers cure once a layer right after a layer height levelling step while other publications reported an additional "pinning" step prior levelling. Some researchers did not implement a layer levelling step, instead the droplets are cured immediately upon drop impact. A sophisticated curing strategy could increase the achievable resolution, geometrical accuracy and surface properties by controlling drop spreading and the merging of adjacent droplets.

Combining more than one material in the printing process will add further challenges originating from the material combination. For example, the materials may need different curing conditions or strategies. In another case one material may be cured by UV exposure while the other is cured by heat, but the heat adversely affects the first material, causing delamination, or changes in shape/size, or diminishes its strength. The possibility of such situations requires that curing strategies need to be known and considered at the design stage when selection of materials is taking place.

9.4. 3D/4D multi-material printing

Material jetting still faces many serious challenges in the production of intricate, multi-material high quality components. Printed parts may be subject to a lack of stability, particularly at interfaces when more than one material is used to manufacture a complex item. This issue requires attention when the strength and durability of the component is a major consideration. Indeed, the lack of mechanical reliability is a major restriction on the industrial application of multi-material inkjet-based 3D/4D printing. Research into this aspect of material jetting would be a step towards a major advance in development. Material jetting capabilities should be extended to fulfill the requirements for a wide range of 3D and 4D applications for example micro-mechanical systems, lab-on-chip for biomedical, environmental or chemical application, and smart devices. Furthermore, it is of great importance to proof that material jetting is capable of manufacturing advanced systems with the same performance and functionality as conventional system.

10. Conclusions

From the above review of research and developmental work related

to material jetting and inkjet printing, it is not difficult to infer that there is considerable attention being given by researchers and manufacturers to further develop the material jetting process.

Following are specific insights that can be concluded based on the conducted review.

- UV-curable inks are reported to have several advantages such as quick curing, no evaporation of carrier required, hence no significant reduction of layer height, and no nozzle drying issues, which make them well-suited for material jetting. However currently available UV-curables are still facing limitation in applications due to the inherently poor mechanical and thermal performances of the materials. Moroever, the migration of hazardous substances (monomer, photoinitiator) of poorly cured components might restrict its applicability in health- or food-related industry.
- In order to improve the functionality of jettable inks both more advanced materials with higher load of polymers or particles and printheads supporting high-viscous inks are to be developed.
- The jettability criterion based on the dimensionless Ohnesorge number, defined over a decade ago for Newtonian fluid, has been introduced. Multiple works observed differences in jetting and drop impact behavior between Newtonian and viscoelastic fluid and some studies proposed further dimensionless numbers such as Weissenberg number or elasticity number, etc. To date, a clear jettability criteria for viscoelastic fluid is still missing, even though numerous measurement equipment for gauging the viscoelasticity of inks at high frequency and high shear rate conditions are available.
- Precise and stable drop formation based on optimized waveform have been widely reported, albeit the development of advanced waveform for newly developed inks are still very time-consuming and could be accelerated for instance by combining drop-watching and AI techniques.
- Several studies on modification of droplet/substrate (or previous cured layer) interaction are analyzed for enhanced high-resolution material jetting process. With its ability to selectively control the drop spreading behavior, plasma-treatment has been concluded to be a promising technique to achieve highly accurate printing, and thus further investigations are highly recommended.
- The review of existing MJ systems revealed that a layer levelling step before the curing could be deployed, while other systems cure immediately upon droplet deposition without levelling the layer. Other studies implemented a "pinning" step, a slight curing to prevent further droplet spread, prior to layer levelling. However, the optimum curing strategy for jettable materials is yet to be further determined.
- Commonly occurring issues in material jetting such as shrinkage, layer height inconsistency, oxygen inhibition and gas dissolvement in the fluid are outlined and existing and potential solutions for mitigating these problems such as ink recirculation, in-loop layer height correction, layer levelling device, curing at inert environment, etc. are pointed out.
- Material jetting has shown high potential as a key enabling technology for a wide range of applications ranging from producing printed electronics, components for chemical, biological and pharmaceutical purposes, and smart devices and microsystems for 3D and 4D applications.

In order to satisfy the growing demand for precise and high-resolution 3D and 4D printing in industry and thereby to facilitate full industrial adoption of material jetting, it is important to extend the frontiers of existing material jetting technology and understand the complete fabrication process. Significant improvements over the entire process chain of material jetting are needed to achieve broader industrial implementation. This comprehensive review paper should offer researchers and engineers operating material jetting printers the opportunity to learn about the most relevant aspects of material jetting and

its advanced applications which, hopefully also help to pave the way to further advance this auspicious manufacturing technology and to expand the number of advanced applications in MJ.

CRediT authorship contribution statement

Steffen G. Scholz: Writing – review & editing, Project administration, Funding acquisition. **Jan C. Janhsen:** Writing – review & editing, Supervision. **Oliver Refle:** Writing – review & editing, Project administration. **Veit Hagenmeyer:** Writing – review & editing. **Ahmed Elkaseer:** Writing – review & editing, Writing – original draft, Visualization, Investigation, Conceptualization. **Karin J. Chen:** Writing – review & editing, Writing – original draft, Visualization, Investigation, Conceptualization.

Declaration of Competing Interest

The authors declare that they have no known competing financial interests or personal relationships that could have appeared to influence the work reported in this paper.

Data Availability

No data was used for the research described in the article.

References

[1] W.-H. Chou, A. Gamboa, J.O. Morales, Inkjet printing of small molecules, biologics, and nanoparticles, Int. J. Pharm. 600 (2021) 120462, https://doi.org/10.1016/j.ijpharm.2021.120462.

[2] S.E. Evans, T. Harrington, M.C. Rodriguez Rivero, E. Rognin, T. Tuladhar, R. Daly, 2D and 3D inkjet printing of biopharmaceuticals – a review of trends and future perspectives in research and manufacturing, Int. J. Pharm. 599 (2021), 120443, https://doi.org/10.1016/j.ijpharm.2021.120443.

[3] N. Li, D. Qiao, S. Zhao, Q. Lin, B. Zhang, F. Xie, 3D printing to innovate biopolymer materials for demanding applications: a review, Mater. Today Chem. 20 (2021), 100459, https://doi.org/10.1016/j.mtchem.2021.100459.

[4] D. Mohan, Z.K. Teong, A.N. Bakir, M.S. Sajab, H. Kaco, Extending cellulose-based polymers application in additive manufacturing technology: a review of recent approaches, Polymers 12 (2020), https://doi.org/10.3390/polym12091876.

[5] T. Tilford, S. Stoyanov, J. Braun, J.C. Janhsen, M.K. Patel, C. Bailey, Comparative reliability of inkjet-printed electronics packaging, IEEE Trans. Compon. Packag Manufact Technol. 11 (2021) 351–362, https://doi.org/10.1109/TCPMT.2021.3049952.

[6] S.H. Ko, J. Chung, N. Hotz, K.H. Nam, C.P. Grigoropoulos, Metal nanoparticle direct inkjet printing for low-temperature 3D micro metal structure fabrication, J. Micromech. Micro 20 (2010), 125010, https://doi.org/10.1088/0960-1317/20/12/125010.

[7] R. Magazine, B. van Bochove, S. Borandeh, J. Seppälä, 3D inkjet-printing of photo-crosslinkable resins for microlens fabrication, Addit. Manuf. 50 (2022), 102534, https://doi.org/10.1016/j.addma.2021.102534.

[8] I.F. Ituarte, N. Boddeti, V. Hassani, M.L. Dunn, D.W. Rosen, Design and additive manufacture of functionally graded structures based on digital materials, Addit. Manuf. 30 (2019), 100839, https://doi.org/10.1016/j.addma.2019.100839.

[9] M. Mikolajek, A. Friederich, C. Kohler, M. Rosen, A. Rathjen, K. Krüger, J. R. Binder, Direct inkjet printing of dielectric ceramic/polymer composite thick films, Adv. Eng. Mater. 17 (2015) 1294–1301, https://doi.org/10.1002/adem.201400451.

[10] A. Aghaei, N. Bochud, G. Rosi, Q. Grossman, D. Ruffoni, S. Naili, Ultrasound characterization of bioinspired functionally graded soft-to-hard composites: Experiment and modeling, J. Acoust. Soc. Am. 151 (2022) 1490, https://doi.org/10.1121/10.0009630.

[11] M.A. Shah, D.-G. Lee, B.-Y. Lee, S. Hur, Classifications and applications of inkjet printing technology: a review, IEEE Access 9 (2021) 140079–140102, https://doi.org/10.1109/ACCESS.2021.3119219.

[12] J.P. Moore, C.B. Williams, Fatigue properties of parts printed by PolyJet material jetting, Rapid Prototyp. J. 21 (2015) 675–685, https://doi.org/10.1108/RPJ-03-2014-0031.

[13] 3D Systems, MultiJet Printing: What Is MultiJet Printing? https://www.3dsystems.com/multi-jet-printing (accessed 2 May 2022).

[14] American Society for Testing and Materials, ISO/ASTM52900:21 Additive manufacturing — General principles — Fundamentals and vocabulary, 2021.

[15] S. Magdassi, The chemistry of inkjet inks, World Scientific Pub. Co, Singapore, Hackensack, N.J, 2010.

[16] O. Gülcan, K. Günaydın, A. Tamer, The state of the art of material jetting-a critical review, Polymers 13 (2021), https://doi.org/10.3390/polym13162829.

[17] P.-A. Högström, S. Karlsson, U.W. Gedde, Effect of aging on the mechanical properties of UV curable optical fiber coatings, Int. J. Polym. Mater. Polym. Biomater. 46 (2000) 403–421, https://doi.org/10.1080/00914030008033884.

[18] Cubicure, Materials Overview, 2022. https://cubicure.com/en/products/materials/.

[19] Formlabs, Formlabs Material Library. https://formlabs.com/materials/ (accessed 11 October 2022).

[20] Henkel, Loctite 3D Materials. https://www.loctiteam.com/materials/ (accessed 11 October 2022).

[21] Stratasys Ltd, Materials. https://www.stratasys.com/en/materials/materials-catalog/polyjet-materials/?filter=MT_PolyJet (accessed 11 October 2022).

[22] 3D Systems, Material Finder. https://www.3dsystems.com/material-finder (accessed 11 October 2022).

[23] 3Dmensionals, Lehvoss Luvocom 3F PEEK 9581 NT Filament. https://www.3dmensionals.de/lehvoss-luvocom-3f-peek-9581-nt-filament (accessed 11 October 2022).

[24] EOS, Plastic 3D Printing. https://www.eos.info/en/additive-manufacturing/3d-printing-plastic (accessed 11 October 2022).

[25] Intamsys, Engineering Materials. https://www.intamsys.com/materials/#Engineering-Materials (accessed 11 October 2022).

[26] R. Walczak, K. Adamski, D. Lizanets, Inkjet 3D printed check microvalve, J. Micromech. Micro 27 (2017) 47002, https://doi.org/10.1088/1361-6439/aa6152.

[27] N.K. Pendyala, S. Magdassi, L. Etgar, Fabrication of perovskite solar cells with digital control of transparency by inkjet printing, ACS Appl. Mater. Interfaces 13 (2021) 30524–30532, https://doi.org/10.1021/acsami.1c04407.

[28] I. Marasco, G. Niro, V.M. Mastronardi, F. Rizzi, A. D'Orazio, M. de Vittorio, M. Grande, A compact evolved antenna for 5G communications, Sci. Rep. 12 (2022) 10327, https://doi.org/10.1038/s41598-022-14447-9.

[29] A. Lion, R.D. Wildman, M.R. Alexander, C.J. Roberts, Customisable tablet printing: the development of multimaterial hot melt inkjet 3D printing to produce complex and personalised dosage forms, Pharmaceutics 13 (2021), https://doi.org/10.3390/pharmaceutics13101679.

[30] X. Wang, M. Zhang, L. Zhang, J. Xu, X. Xiao, X. Zhang, Inkjet-printed flexible sensors: from function materials, manufacture process, and applications perspective, Mater. Today Commun. 31 (2022), 103263, https://doi.org/10.1016/j.mtcomm.2022.103263.

[31] S. Meker, O. Halevi, H. Chin, T.N. Sut, J.A. Jackman, E.-L. Tan, M.G. Potroz, N.-J. Cho, Inkjet-printed phospholipid bilayers on titanium oxide surfaces: towards functional membrane biointerfaces, Membranes 12 (2022), https://doi.org/10.3390/membranes12040361.

[32] P. Pallavicini, G. Chirico, A. Taglietti, Harvesting light to produce heat: photothermal nanoparticles for technological applications and biomedical devices, Chemistry 27 (2021) 15361–15374, https://doi.org/10.1002/chem.202102123.

[33] M. Linke, T. Genco, R. Lammering, Experimental investigations on the mechanical damage behavior of multifucntional composites with printed electronics, 2019, pp. 421–432.

[34] W. Zapka (Ed.), Handbook of industrial inkjet printing: A full system approach Volume 1 & 2, Wiley-VCH, Weinheim, 2018.

[35] H.W. Tan, N. Saengchairat, G.L. Goh, J. An, C.K. Chua, T. Tran, Induction sintering of silver nanoparticle inks on polyimide substrates, Adv. Mater. Technol. 5 (2020), 1900897, https://doi.org/10.1002/admt.201900897.

[36] D. Kim, A. Hussain, H.-L. Lee, Y.-J. Moon, J. Hwang, S.-J. Moon, Stepwise current increment sintering of silver nanoparticle structures, Crystals 11 (2021) 1264, https://doi.org/10.3390/cryst11101264.

[37] HERAEUS NOBLELIGHT, The 'Process Window' of UV-Cured Inkjet Printing. Heraeus Whitepaper.

[38] N. Caiger, Industrial Application of UV-Curing Jet Inks, 2001, pp. 161–164.

[39] Y. Qiu, G. Li, Q. Zhang, C. Tan, D. Xiang, Study on migration of two acrylate monomers in plastic food contact materials, IOP Conf. Ser.: Earth Environ. Sci. 657 (2021) 12036, https://doi.org/10.1088/1755-1315/657/1/012036.

[40] R. Bail, A. Patel, H. Yang, C.M. Rogers, F. Rose, J.I. Segal, S.M. Ratchev, The effect of a type I photoinitiator on cure kinetics and cell toxicity in projection-microstereolithography, Procedia CIRP 5 (2013) 222–225, https://doi.org/10.1016/j.procir.2013.01.044.

[41] J.B. Scarsella, N. Zhang, T.G. Hartman, Identification and migration studies of photolytic decomposition products of UV-photoinitiators in food packaging, Molecules 24 (2019), https://doi.org/10.3390/molecules24193592.

[42] I. Francisco, A.B. Paula, M. Ribeiro, F. Marques, R. Travassos, C. Nunes, F. Pereira, C.M. Marto, E. Carrilho, F. Vale, The biological effects of 3D resins used in orthodontics: a systematic review, Bioengineering 9 (2022), https://doi.org/10.3390/bioengineering9010015.

[43] T. Puskar, B. Trifkovic, T. Djurovic-Koprivica, V. Kojic, A. Jevremovic, S. Mirkovic, D. Eggbeer, In vitro cytotoxicity assessment of the 3D printed polymer based epoxy resin intended for use in dentistry, VSP 76 (2019) 502–509, https://doi.org/10.2298/VSP170721127P.

[44] P.A. Leggat, U. Kedjarune, Toxicity of methyl methacrylate in dentistry, Int. Dent. J. 53 (2003) 126–131, https://doi.org/10.1111/j.1875-595X.2003.tb00736.x.

[45] R. Bongiovanni, S.D. Vacche, A. Vitale, Photoinduced processes as a way to sustainable polymers and innovation in polymeric materials, Polymers 13 (2021), https://doi.org/10.3390/polym13142293.

[46] M. Mohamed, H. Mohamed, M. Moustafa, A. Eid, A comparative study of ultraviolet and electron beam irradiation on acrylate coatings, Egypt. J. Chem. 0 (2019) 0, https://doi.org/10.21608/ejchem.2019.15990.1966.

[47] J.-P. Fouassier, Photoinitiation, photopolymerization, and photocuring: fundamentals and applications, Hanser (1995).

[48] K. Balani, Biosurfaces: A materials science and engineering perspective, ACerS–Wiley, Hoboken, New Jersey, 2014.

[49] E. Saleh, P. Woolliams, B. Clarke, A. Gregory, S. Greedy, C. Smartt, R. Wildman, I. Ashcroft, R. Hague, P. Dickens, C. Tuck, 3D inkjet-printed UV-curable inks for multi-functional electromagnetic applications, Addit. Manuf. 13 (2017) 143–148, https://doi.org/10.1016/j.addma.2016.10.002.

[50] D. McCoul, S. Rosset, S. Schlatter, H. Shea, Inkjet 3D printing of UV and thermal cure silicone elastomers for dielectric elastomer actuators, Smart Mater. Struct. 26 (2017), 125022, https://doi.org/10.1088/1361-665X/aa9695.

[51] J.-H. Lee, J.-H. Kim, K.-T. Hwang, H.-J. Hwang, K.-S. Han, Digital inkjet printing in three dimensions with multiple ceramic compositions, J. Eur. Ceram. Soc. 41 (2021) 1490–1497, https://doi.org/10.1016/j.jeurceramsoc.2020.09.044.

[52] J.E. Fromm, Numerical calculation of the fluid dynamics of drop-on-demand jets, IBM J. Res. Dev. 28 (1984) 322–333, https://doi.org/10.1147/rd.283.0322.

[53] B. Derby, Inkjet printing of functional and structural materials: fluid property requirements, feature stability, and resolution, Annu. Rev. Mater. Res. 40 (2010) 395–414, https://doi.org/10.1146/annurev-matsci-070909-104502.

[54] D. Lohse, Fundamental fluid dynamics challenges in inkjet printing, Annu. Rev. Fluid Mech. 54 (2022) 349–382, https://doi.org/10.1146/annurev-fluid-022321-114001.

[55] S.-H. Kang, et al., Analysis of drop-on-demand piezo inkjet performance, Phys. Fluids 32 (2020) 22007, https://doi.org/10.1063/1.5142023.

[56] N. Reis, B. Derby, Ink jet deposition of ceramic suspensions: modeling and experiments of droplet formation, MRS Proc. 625 (2000), https://doi.org/10.1557/PROC-625-117.

[57] D. Jang, D. Kim, J. Moon, Influence of fluid physical properties on ink-jet printability, Langmuir 25 (2009) 2629–2635, https://doi.org/10.1021/la900059m.

[58] C.D. Stow, M.G. Hadfield, An experimental investigation of fluid flow resulting from the impact of a water drop with an unyielding dry surface, Proc. R. Soc. Lond. A 373 (1981) 419–441.

[59] F.R. Smith, N.C. Buntsma, D. Brutin, Roughness influence on human blood drop spreading and splashing, Langmuir 34 (2018) 1143–1150, https://doi.org/10.1021/acs.langmuir.7b02718.

[60] S. Jung, S.D. Hoath, I.M. Hutchings, The role of viscoelasticity in drop impact and spreading for inkjet printing of polymer solution on a wettable surface, Microfluid Nanofluid 14 (2013) 163–169, https://doi.org/10.1007/s10404-012-1034-3.

[61] Y. Son, C. Kim, Spreading of inkjet droplet of non-Newtonian fluid on solid surface with controlled contact angle at low Weber and Reynolds numbers, J. Non-Newton. Fluid Mech. 162 (2009) 78–87, https://doi.org/10.1016/j.jnnfm.2009.05.009.

[62] Z. Du, Y. Lin, R. Xing, X. Cao, X. Yu, Y. Han, Controlling the polymer ink's rheological properties and viscoelasticity to suppress satellite droplets, Polymer 138 (2018) 75–82, https://doi.org/10.1016/j.polymer.2018.01.052.

[63] N. Reis, C. Ainsley, B. Derby, Viscosity and acoustic behavior of ceramic suspensions optimized for phase-change ink-jet printing, J. Am. Ceram. Soc. 88 (2005) 802–808, https://doi.org/10.1111/j.1551-2916.2005.00138.x.

[64] H. Dong, W.W. Carr, J.F. Morris, An experimental study of drop-on-demand drop formation, Phys. Fluids 18 (2006) 72102, https://doi.org/10.1063/1.2217929.

[65] J. Dinic, V. Sharma, Power laws dominate shear and extensional rheology response and capillary-driven pinching dynamics of entangled hydroxyethyl cellulose (HEC) solutions, Macromolecules 53 (2020) 3424–3437, https://doi.org/10.1021/acs.macromol.0c00077.

[66] X. Wang, W.W. Carr, D.G. Bucknall, J.F. Morris, High-shear-rate capillary viscometer for inkjet inks, Rev. Sci. Instrum. 81 (2010) 65106, https://doi.org/10.1063/1.3449478.

[67] A.U. Khan, N. Mahmood, A.A. Bazmi, Direct comparison between rotational and extrusion rheometers, Mat. Res 12 (2009) 477–481, https://doi.org/10.1590/S1516-14392009000400017.

[68] RheoSense, m-VROC Viscometer: Controlled Shear Rates and Small Samples. https://www.rheosense.com/products/viscometers/m-vroc (accessed 10 March 2021).

[69] M.R. Mackley, R.T.J. Marshall, J.B.A.F. Smeulders, The multipass rheometer, J. Rheol. 39 (1995) 1293–1309, https://doi.org/10.1122/1.550637.

[70] D.C. Vadillo, T.R. Tuladhar, A.C. Mulji, S. Jung, S.D. Hoath, M.R. Mackley, Evaluation of the inkjet fluid's performance using the "Cambridge Trimaster" filament stretch and break-up device, J. Rheol. 54 (2010) 261–282, https://doi.org/10.1122/1.3302451.

[71] Y. Wang, W. Yang, Q. Wang, K. Liu, C. Wang, Q. Chang, The rheological performance of aqueous ceramic ink described based on the modified Windhab model, Mater. Res. Express 7 (2020) 75103, https://doi.org/10.1088/2053-1591/aba507.

[72] F.D.C. Siacor, Q. Chen, J.Y. Zhao, L. Han, A.D. Valino, E.B. Taboada, E.B. Caldona, R.C. Advincula, On the additive manufacturing (3D printing) of viscoelastic materials and flow behavior: from composites to food manufacturing, Addit. Manuf. 45 (2021), 102043, https://doi.org/10.1016/j.addma.2021.102043.

[73] Z. Zhang, Y. Jin, J. Yin, J. Xu, R. Xiong, K. Christensen, B.R. Ringeisen, D.B. Chrisey, Y. Huang, Evaluation of bioink printability for bioprinting applications, Appl. Phys. Rev. 5 (2018) 41304, https://doi.org/10.1063/1.5053979.

[74] G.H. McKinley, Dimensionless Groups For Understanding Free Surface Flows of Complex Fluids. HML Report Number 05-P-05, seventhfourth ed., 2005.

[75] J.J. Crassous, R. Régisser, M. Ballauff, N. Willenbacher, Characterization of the viscoelastic behavior of complex fluids using the piezoelastic axial vibrator, J. Rheol. 49 (2005) 851–863, https://doi.org/10.1122/1.1917843.

[76] H. Yoo, C. Kim, Generation of inkjet drop of particulate gel, Korea-Aust. Rheol. J. 27 (2015) 189–196, https://doi.org/10.1007/s13367-015-0019-7.

[77] K.-H. Schweikart, B. Fechner, H.-T. Macholdt, Dynamic Surface Tension: A Key Parameter for Excellent Ink Jet Preparations.

[78] B. Stückrad, W.J. Hiller, T.A. Kowalewski, Measurement of dynamic surface tension by the oscillating droplet method, Exp. Fluids 15- 15 (1993) 332–340, https://doi.org/10.1007/BF00223411.

[79] E.I. Franses, O.A. Basaran, C.-H. Chang, Techniques to measure dynamic surface tension, Curr. Opin. Colloid Interface Sci. 1 (1996) 296–303, https://doi.org/10.1016/S1359-0294(96)80018-5.

[80] KRÜSS GmbH, Dynamic surface tension, 2021. https://www.kruss-scientific.com/en/know-how/glossary/dynamic-surface-tension (accessed 2 March 2021).

[81] SITA Messtechnik GmbH, Bubble pressure method for measuring the surface tension, 2020. ⟨https://www.sita-process.com/information-service/process-parameter-surface-tension/bubble-pressure-method-for-measuring-the-surface-tension/⟩ (accessed 2 March 2021).

[82] V.B. Fainerman, R. Miller, P. Joos, The measurement of dynamic surface tension by the maximum bubble pressure method, Colloid Polym. Sci. 272 (1994) 731–739, https://doi.org/10.1007/BF00659287.

[83] Z. Zhou, L. Ruiz Cantu, X. Chen, M.R. Alexander, C.J. Roberts, R. Hague, C. Tuck, D. Irvine, R. Wildman, High-throughput characterization of fluid properties to predict droplet ejection for three-dimensional inkjet printing formulations, Addit. Manuf. 29 (2019), 100792, https://doi.org/10.1016/j.addma.2019.100792.

[84] E.Mariano Freire, Ink jet printing technology (CIJ/DOD), in: Digital Printing of Textiles, Elsevier, 2006, pp. 29–52.

[85] O. Oktavianty, T. Kyotani, S. Haruyama, K. Kaminishi, New actuation waveform design of DoD inkjet printer for single and multi-drop ejection method, Addit. Manuf. 25 (2019) 522–531, https://doi.org/10.1016/j.addma.2018.12.008.

[86] K.-S. Kwon, W. Kim, A waveform design method for high-speed inkjet printing based on self-sensing measurement, Sens. Actuators A: Phys. 140 (2007) 75–83, https://doi.org/10.1016/j.sna.2007.06.010.

[87] H. Dong, W.W. Carr, J.F. Morris, Visualization of drop-on-demand inkjet: Drop formation and deposition, Rev. Sci. Instrum. 77 (2006) 85101, https://doi.org/10.1063/1.2234853.

[88] N. Thakur, H. Murthy, Simulation study of droplet formation in inkjet printing using ANSYS FLUENT, J. Phys.: Conf. Ser. 2161 (2022) 12026, https://doi.org/10.1088/1742-6596/2161/1/012026.

[89] Y. Zhang, G. Hu, Y. Liu, J. Wang, G. Yang, D. Li, Suppression and Utilization of Satellite Droplets in Inkjet Printing: A Review, Processes 10 (2022) 932, https://doi.org/10.3390/pr10050932.

[90] H. Yoo, C. Kim, Generation of inkjet droplet of non-Newtonian fluid, Rheol. Acta 52 (2013) 313–325, https://doi.org/10.1007/s00397-013-0688-4.

[91] J.D. Ferry. Viscoelastic properties of polymer solutions, John Wiley & Sons, 1980.

[92] H.J. Shore, G.M. Harrison, The effect of added polymers on the formation of drops ejected from a nozzle, Phys. Fluids 17 (2005) 33104, https://doi.org/10.1063/1.1850431.

[93] R.P. Mun, J.A. Byars, D.V. Boger, The effects of polymer concentration and molecular weight on the breakup of laminar capillary jets, J. Non-Newton. Fluid Mech. 74 (1998) 285–297, https://doi.org/10.1016/S0377-0257(97)00074-8.

[94] H. Onuki, Y. Oi, Y. Tagawa, Microjet generator for highly viscous fluids, Phys. Rev. Appl. 9 (2018), https://doi.org/10.1103/PhysRevApplied.9.014035.

[95] U. Sen, C. Datt, T. Segers, H. Wijshoff, J.H. Snoeijer, M. Versluis, D. Lohse, The retraction of jetted slender viscoelastic liquid filaments, J. Fluid Mech. 929 (2021), https://doi.org/10.1017/jfm.2021.855.

[96] C. Gao, T. Xing, G. Chen, Research on micro mechanism of water-based disperse ink and optimization of driving waveform for inkjet ink, Colloids Surf. A

[97] Physicochem. Eng. Asp. 606 (2020), 125237, https://doi.org/10.1016/j.colsurfa.2020.125237.

[97] J. Wang, J. Huang, J. Peng, J. Zhang, Piezoelectric print-head drive-waveform optimization method based on self-sensing, Sens. Actuators A: Phys. 299 (2019), 111617, https://doi.org/10.1016/j.sna.2019.111617.

[98] A.H. Hamad, M.I. Salman, A. Mian, Effect of driving waveform on size and velocity of generated droplets of nanosilver ink (Smartink, Manuf. Lett. 24 (2020) 14–18, https://doi.org/10.1016/j.mfglet.2020.03.001.

[99] Z. Du, X. Yu, Y. Han, Inkjet printing of viscoelastic polymer inks, Chin. Chem. Lett. 29 (2018) 399–404, https://doi.org/10.1016/j.cclet.2017.09.031.

[100] A.B. Aqeel, M. Mohasan, P. Lv, Y. Yang, H. Duan, Effects of the actuation waveform on the drop size reduction in drop-on-demand inkjet printing, Acta Mech. Sin. 36 (2020) 983–989, https://doi.org/10.1007/s10409-020-00991-y.

[101] P.C. Duineveld, J.F. Dijksman, Ultra small droplet generation in inkjet printing by higher order meniscus oscillations, print4fab 34 (2018) 147–150, https://doi.org/10.2352/ISSN.2169-4451.2018.34.147.

[102] B. Snyder, M. Yang, S. Singhal, O. Abed, S.V. Sreenivasan, Automated tuning of high-order waveforms for picoliter resolution jetting of rheologically challenging materials, Precis. Eng. 56 (2019) 143–155, https://doi.org/10.1016/j.precisioneng.2018.11.009.

[103] A.B. Aqeel, M. Mohasan, P. Lv, Y. Yang, H. Duan, Effects of nozzle and fluid properties on the drop formation dynamics in a drop-on-demand inkjet printing, Appl. Math. Mech.-Engl. Ed (2019) 1239–1254, https://doi.org/10.1007/s10483-019-2514-7.

[104] J.C. Miers, W. Zhou, Droplet formation at megahertz frequency, AIChE J. 63 (2017) 2367–2377, https://doi.org/10.1002/aic.15578.

[105] S.-H. Kang, S. Kim, J.W. Lim, D.K. Sohn, H.S. Ko, Study on fall velocity of continuously ejected micro inkjet droplet, J. Mech. Sci. Technol. 34 (2020) 3311–3315, https://doi.org/10.1007/s12206-020-0723-1.

[106] H. Wijshoff, Drop dynamics in the inkjet printing process, Curr. Opin. Colloid Interface Sci. 36 (2018) 20–27, https://doi.org/10.1016/j.cocis.2017.11.004.

[107] A. Fraters, M. Rump, R. Jeurissen, M. van den Berg, Y. de Loore, H. Reinten, H. Wijshoff, D. van der Meer, D. Lohse, M. Versluis, T. Segers, Meniscus oscillations driven by flow focusing lead to bubble pinch-off and entrainment in a piezoacoustic inkjet nozzle, Phys. Rev. Appl. 16 (2021) 44052, https://doi.org/10.1103/PhysRevApplied.16.044052.

[108] Y.-L. Cheng, T.-W. Tseng, Study on driving waveform design process for multi-nozzle piezoelectric printhead in material-jetting 3D printing, RPJ 27 (2021) 1172–1180, https://doi.org/10.1108/RPJ-05-2019-0120.

[109] A. Fraters, M. van den Berg, Y. de Loore, H. Reinten, H. Wijshoff, D. Lohse, M. Versluis, T. Segers, Inkjet nozzle failure by heterogeneous nucleation: bubble entrainment, cavitation, and diffusive growth, Phys. Rev. Appl. 12 (2019) 64019, https://doi.org/10.1103/PhysRevApplied.12.064019.

[110] T. Jiao, Q. Lian, T. Zhao, H. Wang, Influence of ink properties and voltage parameters on piezoelectric inkjet droplet formation, Appl. Phys. A 127 (2021), https://doi.org/10.1007/s00339-020-04151-8.

[111] Ruizhi Shi Jilei Chao, Yanling Guo Fuqiang Chu, Siyang Liu, Preparation and the Properties of Epoxy Acrylic Resin for Inkjet Printing Ink, in: Dou Zhao (Ed.), Advanced Graphic Communication, Printing and Packaging Technology, Springer Singapore, 2020, pp. 602–609.

[112] F. Marangon, W.K. Hsiao, G. Brenn, C. Planchette, Satellite drop formation during piezo-based inkjet printing, 29th Conf. Liq. At. Spray. Syst., Paris, Fr. (2019).

[113] G. Wang, C. Zhu, T. Fu, Y. Ma, Formation mechanism and criterion of tail satellite droplets for moving droplet in microchannel, Chem. Eng. Sci. 238 (2021), 116607, https://doi.org/10.1016/j.ces.2021.116607.

[114] K. Zhang, K. Fang, M.N. Bukhari, R. Xie, Y. Song, Z. Tang, X. Zhang, The effect of ink drop spreading and coalescing on the image quality of printed cotton fabric, Cellulose 27 (2020) 9725–9736, https://doi.org/10.1007/s10570-020-03446-6.

[115] N.C. Martins, S. Fateixa, T. Fernandes, H.I. Nogueira, T. Trindade, Inkjet printing of ag and polystyrene nanoparticle emulsions for the one-step fabrication of hydrophobic paper-based surface-enhanced raman scattering substrates, ACS Appl. Nano Mater. 4 (2021) 4484–4495, https://doi.org/10.1021/acsanm.1c00112.

[116] H.R. Tiyyagura, P. Majerič, M. Bračič, I. Anžel, R. Rudolf, Gold inks for inkjet printing on photo paper: complementary characterisation, Nanomaterials 11 (2021) 599, https://doi.org/10.3390/nano11030599.

[117] X. Wan, X. Miao, J. Yao, S. Wang, F. Shao, S. Xiao, R. Zhan, K. Chen, X. Zeng, X. Gu, J. Xu, In situ ultrafast and patterned growth of transition metal dichalcogenides from inkjet-printed aqueous precursors, Adv. Mater. 33 (2021), e2100260, https://doi.org/10.1002/adma.202100260.

[118] S. Dudala, S. Srikanth, S.K. Dubey, A. Javed, S. Goel, Rapid Inkjet-Printed Miniaturized Interdigitated Electrodes for Electrochemical Sensing of Nitrite and Taste Stimuli, Micromachines 12 (2021) 1037, https://doi.org/10.3390/mi12091037.

[119] M.A. Riheen, T.K. Saha, P.K. Sekhar, Inkjet printing on PET substrate, J. Electrochem. Soc. 166 (2019) B3036–B3039, https://doi.org/10.1149/2.0091909jes.

[120] G. Tomaszewski, P. Jankowski-Mihułowicz, J. Potencki, A. Pietrikova, P. Lukacs, Inkjet-printed HF antenna made on PET substrate, Microelectron. Reliab. 129 (2022), 114473, https://doi.org/10.1016/j.microrel.2021.114473.

[121] S. Uzun, M. Schelling, K. Hantanasirisakul, T.S. Mathis, R. Askeland, G. Dion, Y. Gogotsi, Additive-Free Aqueous MXene Inks for Thermal Inkjet Printing on Textiles, Small 17 (2021), 2006376, https://doi.org/10.1002/smll.202006376.

[122] H.-J. Kim, J.-P. Hong, M.-J. Kim, S.-Y. Kim, J.-H. Kim, D.-J. Kwon, Improving the digital to garment inkjet printing properties of cotton by control the butyl acrylate

content of the surface treatment agent, Appl. Surf. Sci. 583 (2022), 152322, https://doi.org/10.1016/j.apsusc.2021.152322.

[123] Yunnan Fang, Manos M. Tentzeris, Surface Modification of Polyimide Films for Inkjet-Printing of Flexible Electronic Devices, in: S. Rackauskas (Ed.), Flexible Electronics, IntechOpen, 2018.

[124] S.K. Nemani, R.K. Annavarapu, B. Mohammadian, A. Raiyan, J. Heil, M.A. Haque, A. Abdelaal, H. Sojoudi, Surface Modification of Polymers: Methods and Applications, Adv. Mater. Interfaces 5 (2018), 1801247, https://doi.org/10.1002/admi.201801247.

[125] J. Izdebska-Podsiadły, Effect of Plasma Surface Modification on Print Quality of Biodegradable PLA Films, Appl. Sci. 11 (2021) 8245, https://doi.org/10.3390/app11178245.

[126] D.Y. Kim, Y.J. Han, J. Choi, C. Sakong, B.-K. Ju, K.H. Cho, Inkjet printed quantum dot film formed by controlling surface wettability for blue-to-green color conversion, Org. Electron. 84 (2020), 105814, https://doi.org/10.1016/j.orgel.2020.105814.

[127] S. Orazbayev, M. Gabdullin, T. Ramazanov, Z. Askar, Z. Rakhymzhan, Obtaining hydrophobic surfaces in atmospheric pressure plasma, Mater. Today.: Proc. 20 (2020) 335–341, https://doi.org/10.1016/j.matpr.2019.10.071.

[128] H.Y. Park, B.J. Kang, D. Lee, J.H. Oh, Control of surface wettability for inkjet printing by combining hydrophobic coating and plasma treatment, Thin Solid Films 546 (2013) 162–166, https://doi.org/10.1016/j.tsf.2013.03.067.

[129] M. Modic, I. Junkar, A. Vesel, M. Mozetic, Aging of plasma treated surfaces and their effects on platelet adhesion and activation, Surf. Coat. Technol. 213 (2012) 98–104, https://doi.org/10.1016/j.surfcoat.2012.10.026.

[130] Z. Zhai, Q. He, L. Fu, N. Liu, X. Liu, B. Jiang, M. Zhou, Effect of plasma treatment parameters on the interfacial joining strength of overmolded hybrid fiber reinforced thermoplastic composites, J. Appl. Polym. Sci. 139 (2022) 52166, https://doi.org/10.1002/app.52166.

[131] C. Aydemir, B.N. Altay, M. Akyol, Surface analysis of polymer films for wettability and ink adhesion, Color Res Appl. 46 (2021) 489–499, https://doi.org/10.1002/col.22579.

[132] R. Xing, T. Ye, Y. Ding, D. Ma, Y. Han, Formation of low surface energy separators with undercut structures via a full-solution process and its application in inkjet printed matrix of polymer light-emitting diodes, Org. Electron. 10 (2009) 313–319, https://doi.org/10.1016/j.orgel.2008.12.006.

[133] Y. Li, L. Lan, S. Sun, Z. Lin, P. Gao, W. Song, E. Song, P. Zhang, J. Peng, All Inkjet-Printed Metal-Oxide Thin-Film Transistor Array with Good Stability and Uniformity Using Surface-Energy Patterns, ACS Appl. Mater. Interfaces 9 (2017) 8194–8200, https://doi.org/10.1021/acsami.7b00435.

[134] C. Lee, B.J. Kang, J.H. Oh, High-resolution conductive patterns fabricated by inkjet printing and spin coating on wettability-controlled surfaces, Thin Solid Films 616 (2016) 238–246, https://doi.org/10.1016/j.tsf.2016.08.027.

[135] P. Krüger, R. Knes, J. Friedrich, Surface cleaning by plasma-enhanced desorption of contaminants (PEDC), Surf. Coat. Technol. 112 (1999) 240–244, https://doi.org/10.1016/S0257-8972(98)00777-4.

[136] B.J. Kang, Y.S. Kim, Y.W. Cho, J.H. Oh, Effects of plasma surface treatments on inkjet-printed feature sizes and surface characteristics, Micro Eng. 88 (2011) 2355–2358, https://doi.org/10.1016/j.mee.2010.12.045.

[137] C. Zhang, X. Zhang, Nano-modification of plasma treated inkjet printing fabrics, Int. J. Cloth. Sci. Technol. 27 (2015) 159–169, https://doi.org/10.1108/IJCST-07-2013-0078.

[138] A. Pietrikova, P. Lukacs, D. Jakubeczyova, B. Ballokova, J. Potencki, G. Tomaszewski, J. Pekarek, K. Prikrylova, M. Fides, Surface analysis of polymeric substrates used for inkjet printing technology, Circuit World 42 (2016) 9–16, https://doi.org/10.1108/CW-10-2015-0047.

[139] J.P. Fouassier, J. Lalevée, Photoinitiators for Polymer Synthesis: Scope, Reactivity, and Efficiency, Wiley, 2013.

[140] T. Pirman, M. Ocepek, B. Likozar, Radical polymerization of acrylates, methacrylates, and styrene: biobased approaches, mechanism, kinetics, secondary reactions, and modeling, Ind. Eng. Chem. Res. 60 (2021) 9347–9367, https://doi.org/10.1021/acs.iecr.1c01649.

[141] J.V. Crivello, Photoinitiated cationic polymerization, Annu. Rev. Mater. Sci. 13 (1983) 173–190, https://doi.org/10.1146/annurev.ms.13.080183.001133.

[142] C. Decker, T. Nguyen Thi Viet, H. Pham Thi, Photoinitiated cationic polymerization of epoxides, Polym. Int. 50 (2001) 986–997, https://doi.org/10.1002/pi.730.

[143] C. Kutal, P.A. Grutsch, D.B. Yang, A novel strategy for photoinitiated anionic polymerization, Macromolecules 24 (1991) 6872–6873, https://doi.org/10.1021/ma00026a016.

[144] A. Hancock, L. Lin, Challenges of UV curable ink-jet printing inks – a formulator's perspective, Pigment Resin Technol. 33 (2004) 280–286, https://doi.org/10.1108/03699420410560470.

[145] A. Mitchell, U. Lafont, M. Hołyńska, C. Semprimoschnig, Additive manufacturing — a review of 4D printing and future applications, Addit. Manuf. 24 (2018) 606–626, https://doi.org/10.1016/j.addma.2018.10.038.

[146] M.N. Hafsa, M. Ibrahim, S. Sharif, Investment casting using multi-jet modelling patterns: the thermogravimetric analysis of visijet® SR200 UV curable acrylate plastic, IOP Conf. Ser. Mater. Sci. Eng. 50 (2013) 12059, https://doi.org/10.1088/1757-899X/50/1/012059.

[147] 3D Systems, Material SDS. http://infocenter.3dsystems.com/materials/ (accessed 31 December 2021).

[148] Stratasys Ltd, Safety Data Sheets. https://support.stratasys.com/de/Materials/SDS (accessed 31 December 2021).

[149] Stratasys Ltd, VeroVivid Color Family. https://www.stratasys.com/materials/search/verovivid (accessed 4 January 2022).

[150] N. Atsushi, T. Atsushi, K. Shuji, Development of New Cationic UV Curable Inkjet Ink, Pittsburgh, Pennsylvania, IS T Soc. Imaging Sci. Technol. 532–534 (2008) 3.

[151] A.J. Peacock, A. Calhoun, Polymer chemistry: Properties and applications, Hanser, München, 2006.

[152] M.S. Malik, S. Schlögl, M. Wolfahrt, M. Sangermano, Review on UV-induced cationic frontal polymerization of epoxy monomers, Polymers 12 (2020), https://doi.org/10.3390/polym12092146.

[153] P. Prabhakaran, K.-S. Lee, Photo-polymerization, in: M.A. Jafar Mazumder, H. Sheardown, A. Al-Ahmed (Eds.), Functional Polymers, Springer, Cham, 2019, pp. 1–53.

[154] C.T. Sanderson, B.J. Palmer, A. Morgan, M. Murphy, R.A. Dluhy, T. Mize, I. J. Amster, C. Kutal, Classical metallocenes as photoinitiators for the anionic polymerization of an alkyl 2-cyanoacrylate, Macromolecules 35 (2002) 9648–9652, https://doi.org/10.1021/ma0212238.

[155] B.J. Palmer, C. Kutal, R. Billing, H. Hennig, A new photoinitiator for anionic polymerization, Macromolecules 28 (1995) 1328–1329, https://doi.org/10.1021/ma00108a078.

[156] R.B. Paul, J.M. Kelly, D.C. Pepper, C. Long, Photoinduced anionic polymerization of cyanoacrylates using substituted pyridine pentacarbonyl complexes of tungsten or chromium, Polymer 38 (1997) 2011–2014, https://doi.org/10.1016/S0032-3861(96)00965-2.

[157] Y.-H. Wang, P. Wan, Ketoprofen as a photoinitiator for anionic polymerization, Photochem. Photobiol. Sci. Off. J. Eur. Photochem. Assoc. Eur. Soc. Photobiol. 14 (2015) 1120–1126, https://doi.org/10.1039/c4pp00454j.

[158] Palmer Yamaguchi, Wakamatsu Kutal Yang, Ferrocenes as anionic photoinitiators, Macromolecules 31 (1998) 5155–5157, https://doi.org/10.1021/ma980376l.

[159] Y. Yamaguchi, C. Kutal, Benzoyl-substituted ferrocenes: an attractive new class of anionic photoinitiators, Macromolecules 33 (2000) 1152–1156, https://doi.org/10.1021/ma9915982.

[160] M. Bouzrati-Zerelli, M. Frigoli, F. Dumur, B. Graff, J.P. Fouassier, J. Lalevée, Design of novel photobase generators upon violet LEDs and use in photopolymerization reactions, Polymer 124 (2017) 151–156, https://doi.org/10.1016/j.polymer.2017.07.068.

[161] P. Glöckner, Radiation curing: Coatings and printing inks technical basics, applications and trouble shooting, Elsevier Science, Hannover, 2008.

[162] A. Ravve, Principles of Polymer Chemistry, Springer, New York, NY, 1995.

[163] E. Çelik, Additive manufacturing: Science and technology, De Gruyter, Berlin, Boston, 2020.

[164] C. Decker, The use of UV irradiation in polymerization, Polym. Int. 1998 (1998) 133–141.

[165] O. Konuray, A. Sola, J. Bonada, A. Tercjak, A. Fabregat-Sanjuan, X. Fernández-Francos, X. Ramis, Cost-effectively 3D-printed rigid and versatile interpenetrating polymer networks, Mater. (Basel, Switz.) 14 (2021), https://doi.org/10.3390/ma14164544.

[166] Z. Yang, J. Shan, Y. Huang, X. Dong, W. Zheng, Y. Jin, W. Zhou, Preparation and mechanism of free-radical/cationic hybrid photosensitive resin with high tensile strength for three-dimensional printing applications, J. Appl. Polym. Sci. 138 (2021) 49881, https://doi.org/10.1002/app.49881.

[167] Z. Tang, J. Gong, P. Cao, L. Tao, X. Pei, T. Wang, Y. Zhang, Q. Wang, J. Zhang, 3D printing of a versatile applicability shape memory polymer with high strength and high transition temperature, Chem. Eng. J. 431 (2022), 134211, https://doi.org/10.1016/j.cej.2021.134211.

[168] B. Chu, J. He, Z. Wang, L. Liu, X. Li, C.-X. Wu, C. Chen, M. Tu, Proangiogenic peptide nanofiber hydrogel/3D printed scaffold for dermal regeneration, Chem. Eng. J. 424 (2021), 128146, https://doi.org/10.1016/j.cej.2020.128146.

[169] R. Schipani, S. Scheurer, R. Florentin, S.E. Critchley, D.J. Kelly, Reinforcing interpenetrating network hydrogels with 3D printed polymer networks to engineer cartilage mimetic composites, Biofabrication 12 (2020) 35011, https://doi.org/10.1088/1758-5090/ab8708.

[170] M. Du, W. Lu, Y. Zhang, A. Mata, Y. Fang, Natural polymer-sourced interpenetrating network hydrogels: fabrication, properties, mechanism and food applications, Trends Food Sci. Technol. 116 (2021) 342–356, https://doi.org/10.1016/j.tifs.2021.07.031.

[171] T. Borjigin, G. Noirbent, D. Gigmes, P. Xiao, F. Dumur, J. Lalevée, The new LED-sensitive photoinitiators of polymerization: copper complexes in free radical and cationic photoinitiating systems and application in 3D printing, Eur. Polym. J. 162 (2022), 110885, https://doi.org/10.1016/j.eurpolymj.2021.110885.

[172] M. Rahal, B. Graff, J. Toufaily, T. Hamieh, M. Ibrahim-Ouali, F. Dumur, J. Lalevée, Naphthyl-naphthalimides as high-performance visible light photoinitiators for 3d printing and photocomposites synthesis, Catalysts 11 (2021) 1269, https://doi.org/10.3390/catal11111269.

[173] C. Decker, Kinetic study and new applications of UV radiation curing, Macromol. Rapid Commun. 23 (2002) 1067–1093, https://doi.org/10.1002/marc.200290014.

[174] J.W. Kopatz, J. Unangst, A.W. Cook, L.N. Appelhans, Compositional effects on cure kinetics, mechanical properties and printability of dual-cure epoxy/acrylate resins for DIW additive manufacturing, Addit. Manuf. 46 (2021), 102159, https://doi.org/10.1016/j.addma.2021.102159.

[175] Y. He, C.J. Tuck, E. Prina, S. Kilsby, S.D.R. Christie, S. Edmondson, R.J.M. Hague, F.R.A.J. Rose, R.D. Wildman, A new photocrosslinkable polycaprolactone-based ink for three-dimensional inkjet printing, J. Biomed. Mater. Res. B Appl. Biomater. 105 (2017) 1645–1657, https://doi.org/10.1002/jbm.b.33699.

[176] R. Anastasio, W. Peerbooms, R. Cardinaels, L.C.A. van Breemen, Characterization of ultraviolet-cured methacrylate networks: from photopolymerization to

ultimate mechanical properties, Macromolecules 52 (2019) 9220–9231, https://doi.org/10.1021/acs.macromol.9b01439.

[177] J. Pierrel, A. Ibrahim, C. Croutxé-Barghorn, X. Allonas, Effect of the oxygen affected layer in multilayered photopolymers, Polym. Chem. 8 (2017) 4596–4602, https://doi.org/10.1039/C7PY00974G.

[178] K. Taki, Y. Watanabe, T. Tanabe, H. Ito, M. Ohshima, Oxygen concentration and conversion distributions in a layer-by-layer UV-cured film used as a simplified model of a 3D UV inkjet printing system, Chem. Eng. Sci. 158 (2017) 569–579, https://doi.org/10.1016/j.ces.2016.10.050.

[179] P. Zhao, Y. He, G.F. Trindade, M. Baumers, D.J. Irvine, R.J. Hague, I.A. Ashcroft, R.D. Wildman, Modelling the influence of UV curing strategies for optimisation of inkjet based 3D printing, Mater. Des. 208 (2021) 109889, https://doi.org/10.1016/j.matdes.2021.109889.

[180] E. Behroodi, H. Latifi, F. Najafi, A compact LED-based projection microstereolithography for producing 3D microstructures, Sci. Rep. 9 (2019) 19692, https://doi.org/10.1038/s41598-019-56044-3.

[181] J.-W. Choi, E. MacDonald, R. Wicker, Multi-material microstereolithography, Int J. Adv. Manuf. Technol. 49 (2010) 543–551, https://doi.org/10.1007/s00170-009-2434-8.

[182] A. Beer, Grundriss des photometrischen Calcüles, Friedrich Vieweg und Sohn, Braunschweig, 1854.

[183] P.F. Jacobs, Fundamentals of Stereolithography, in: Proceedings for the 1992 International Solid Freeform Fabrication Symposium, Austin, Texas, 1992.

[184] J. Bennett, Measuring UV curing parameters of commercial photopolymers used in additive manufacturing, Addit. Manuf. 18 (2017) 203–212, https://doi.org/10.1016/j.addma.2017.10.009.

[185] S. Jacob, A.B. Nair, V. Patel, J. Shah, 3D printing technologies: recent development and emerging applications in various drug delivery systems, AAPS PharmSciTech 21 (2020) 220, https://doi.org/10.1208/s12249-020-01771-4.

[186] A.C. Uzcategui, A. Muralidharan, V.L. Ferguson, S.J. Bryant, R.R. McLeod, Understanding and improving mechanical properties of 3d printed parts using a dual-cure acrylate-based resin for stereolithography, Adv. Eng. Mater. 20 (2018), https://doi.org/10.1002/adem.201800876.

[187] G. Fei, C. Parra-Cabrera, K. Zhong, M.L. Tietze, K. Clays, R. Ameloot, Scattering model for composite stereolithography to enable resin–filler selection and cure depth control, ACS Appl. Polym. Mater. 3 (2021) 6705–6712, https://doi.org/10.1021/acsapm.1c01519.

[188] V. Tomeckova, J.W. Halloran, Cure depth for photopolymerization of ceramic suspensions, J. Eur. Ceram. Soc. 30 (2010) 3023–3033, https://doi.org/10.1016/j.jeurceramsoc.2010.06.004.

[189] V. Tomeckova, J.W. Halloran, Critical energy for photopolymerization of ceramic suspensions in acrylate monomers, J. Eur. Ceram. Soc. 30 (2010) 3273–3282, https://doi.org/10.1016/j.jeurceramsoc.2010.08.003.

[190] M.K. Alazzawi, S.S. Kondapalli, R.A. Haber, Photocurable alumina and silver suspensions: cure depth in highly agglomerated and dispersed systems, J. Mater. Res 36 (2021) 4275–4286, https://doi.org/10.1557/s43578-021-00398-w.

[191] A. Champion, B. Metral, A.-S. Schuller, C. Croutxé-Barghorn, C. Ley, L. Halbardier, X. Allonas, A simple and efficient model to determine the photonic parameters of a photopolymerizable resin usable in 3D printing, ChemPhotoChem 5 (2021) 839–846, https://doi.org/10.1002/cptc.202100002.

[192] J. Simon, A. Langenscheidt, Curing behavior of a UV-curable inkjet ink: distinction between surface-cure and deep-cure performance, J. Appl. Polym. Sci. 137 (2020) 49218, https://doi.org/10.1002/app.49218.

[193] M.E. Nichols, C.M. Seubert, W.H. Weber, J.L. Gerlock, A simple Raman technique to measure the degree of cure in UV curable coatings, Prog. Org. Coat. 43 (2001) 226–232, https://doi.org/10.1016/S0300-9440(01)00173-4.

[194] A. Palanisamy, B.S. Rao, Photo-DSC and dynamic mechanical studies on UV curable compositions containing diacrylate of ricinoleic acid amide derived from castor oil, Prog. Org. Coat. 60 (2007) 161–169, https://doi.org/10.1016/j.porgcoat.2007.06.002.

[195] Novagard, Understanding UV Curing Options for Industry: WhitePaper, 2020. ⟨https://www.novagard.com/wp-content/uploads/2020/11/Novagard_WhitePaper_UVCuringLampTechnology_v1.0-EmailFile.pdf⟩ (accessed 14 January 2022).

[196] INTERTRONICS, Whitepaper: Moving to UV LED Curing, the 365nm Myth - A Dance between Physics and Chemistry, 2021. ⟨https://www.researchgate.net/publication/352479150_White_Paper_Moving_to_UV_LED_Curing_the_365nm_Myth_-_A_Dance_between_Physics_and_Chemistry⟩ (accessed 14 January 2022).

[197] K. Taki, K. Sawa, Hybrid UV LED device for simulating spectrum of high-pressure mercury lamp: evaluation in UV curing process, J. Photo Sci. Technol. 31 (2018) 753–757, https://doi.org/10.2494/photopolymer.31.753.

[198] World Health Organization Regional Office for Europe, Implementation of the Minamata Convention in the health sector: challenges and opportunities: Information note, 2017.

[199] Y.-L. Cheng, C.-H. Chang, C. Kuo, Experimental study on leveling mechanism for material-jetting-type color 3D printing, Rapid Prototyp. J. 26 (2020) 11–20, https://doi.org/10.1108/RPJ-09-2018-0227.

[200] A. Elkaseer, S. Schneider, Y. Deng, S.G. Scholz, Effect of Process Parameters on the Performance of Drop-On-Demand 3D Inkjet Printing: Geometrical-Based Modeling and Experimental Validation, Polymers 14 (2022), https://doi.org/10.3390/polym14132557.

[201] G. Yang, S. Peng, A. Ridyard, J. Kuta, U.V. LED, curing in inkjet printing applications, Pittsburgh, Pennsylvania, IS T Soc. Imaging Sci. Technol. (2008) 535–537.

[202] W. Zhou, D. Loney, A.G. Fedorov, F.L. Degertekin, D.W. Rosen, Shape evolution of multiple interacting droplets in inkjet deposition, Rapid Prototyp. J. 21 (2015) 373–385, https://doi.org/10.1108/RPJ-12-2013-0131.

[203] C. Mendes-Felipe, D. Patrocinio, J.M. Laza, L. Ruiz-Rubio, J.L. Vilas-Vilela, Evaluation of postcuring process on the thermal and mechanical properties of the Clear02™ resin used in stereolithography, Polym. Test. 72 (2018) 115–121, https://doi.org/10.1016/j.polymertesting.2018.10.018.

[204] X. Feng, Z. Yang, S. Chmely, Q. Wang, S. Wang, Y. Xie, Lignin-coated cellulose nanocrystal filled methacrylate composites prepared via 3D stereolithography printing: mechanical reinforcement and thermal stabilization, Carbohydr. Polym. 169 (2017) 272–281, https://doi.org/10.1016/j.carbpol.2017.04.001.

[205] F. Zareanshahraki, A. Davenport, N. Cramer, C. Seubert, E. Lee, M. Cassoli, X. Wang, Additive manufacturing for automotive applications: mechanical and weathering durability of vat photopolymerization materials, 3D Print. Addit. Manuf. 8 (2021) 302–314, https://doi.org/10.1089/3dp.2020.0244.

[206] X. Chen, I.A. Ashcroft, C.J. Tuck, Y.F. He, R.J.M. Hague, R.D. Wildman, An investigation into the depth and time dependent behavior of UV cured 3D ink jet printed objects, J. Mater. Res 32 (2017) 1407–1420, https://doi.org/10.1557/jmr.2017.4.

[207] Z. Yang, G. Wu, S. Wang, M. Xu, X. Feng, Dynamic postpolymerization of 3D-printed photopolymer nanocomposites: Effect of cellulose nanocrystal and postcure temperature, J. Polym. Sci. Part B: Polym. Phys. 56 (2018) 935–946, https://doi.org/10.1002/polb.24610.

[208] L.F. Vieira, R.A. Paggi, G.V. Salmoria, Thermal and dynamic-mechanical behavior of Fullcure 3D printing resin post-cured by different methods. Boca Raton, Fla, CRC Press/Balkema,, Leiria, Portugal, 2012, pp. 385–388.

[209] Z. Zguris, Formlabs White Paper: How Mechanical Properties of Stereolithography 3D Prints are Affected by UV Curing. ⟨https://formlabs.com/media/upload/How-Mechanical-Properties-of-SLA-3D-Prints-Are-Affected-by-UV-Curing.pdf⟩ (accessed 8 November 2022).

[210] M. Dewaele, E. Asmussen, A. Peutzfeldt, E.C. Munksgaard, A.R. Benetti, G. Finné, G. Leloup, J. Devaux, Influence of curing protocol on selected properties of light-curing polymers: degree of conversion, volume contraction, elastic modulus, and glass transition temperature, Dent. Mater. Off. Publ. Acad. Dent. Mater. 25 (2009) 1576–1584, https://doi.org/10.1016/j.dental.2009.08.001.

[211] D.L. Cohen, H. Lipson, Geometric feedback control of discrete-deposition SFF systems, Rapid Prototyp. J. 16 (2010) 377–393, https://doi.org/10.1108/13552541011065777.

[212] K. Georgieva, D.J. Dijkstra, H. Fricke, N. Willenbacher, Clogging of microchannels by nano-particles due to hetero-coagulation in elongational flow, J. Colloid Interface Sci. 352 (2010) 265–277, https://doi.org/10.1016/j.jcis.2010.08.065.

[213] Q. Huang, J. Zhang, A. Sabbaghi, T. Dasgupta, Optimal offline compensation of shape shrinkage for three-dimensional printing processes, IIE Trans. 47 (2015) 431–441, https://doi.org/10.1080/0740817X.2014.955599.

[214] L. Lu, J. Zheng, S. Mishra, A Model-Based Layer-to-Layer Control Algorithm for Ink-Jet 3D Printing, in: 2014 Proceedings of the ASME 2014 Dynamic Systems and Control Conference (DSCC2014): Volume 2, San Antonio, Texas, USA, American Society of Mechanical Engineers, 2014.

[215] Y. Guo, S. Mishra, A predictive control algorithm for layer-to-layer ink-jet 3D printing, Boston, MA, USA, IEEE, 2016, pp. 833–838.

[216] L. Lu, J. Zheng, S. Mishra, A layer-to-layer model and feedback control of ink-Jet 3-D printing, IEEE/ASME Trans. Mechatron. 20 (2015) 1056–1068, https://doi.org/10.1109/TMECH.2014.2366123.

[217] J. Huang, L.J. Segura, T. Wang, G. Zhao, H. Sun, C. Zhou, Unsupervised learning for the droplet evolution prediction and process dynamics understanding in inkjet printing, Addit. Manuf. 35 (2020) 101197, https://doi.org/10.1016/j.addma.2020.101197.

[218] L.J. Segura, T. Wang, C. Zhou, H. Sun, Online droplet anomaly detection from streaming videos in inkjet printing, Addit. Manuf. 38 (2021), 101835, https://doi.org/10.1016/j.addma.2020.101835.

[219] A. Pugalendhi, R. Ranganathan, M. Chandrasekaran, Effect of process parameters on mechanical properties of VeroBlue material and their optimal selection in PolyJet technology, Int. J. Adv. Manuf. Technol. 108 (2020) 1049–1059, https://doi.org/10.1007/s00170-019-04782-z.

[220] Keyence Deutschland GmbH, Verbesserung der Genauigkeit mittels Inkjet-Technologie: Druckverfahren. https://eb-tec.de/polyjet-keyence/ (accessed 2 May 2022).

[221] Mimaki, 3DUJ-553. ⟨https://www.mimakieurope.com/products/3d/3duj-553/#mimaki-carousel⟩ (accessed 2 May 2022).

[222] K. Hakkaku (MIMAKI ENG CO LTD [JP]) US2021053277 (A1), 2020.

[223] E.M. Kritchman, H. Gothait (OBJET GEOMETRIES LTD [IL]) EP1674243 (A2), 2005.

[224] S. Ikeda, R. Suzaki (KEYENCE CO LTD [JP]) EP2447045 (A2), 2011.

[225] M. Rumbak, E. Napadensky, R. Sarfati, G. Mida (STRATASYS LTD [IL]) WO2019130308 (A1), 2018.

[226] M. Pilkenton, J. Lewman, R. Chartoff, Effect of oxygen on the crosslinking and mechanical properties of a thermoset formed by free-radical photocuring, J. Appl. Polym. Sci. 119 (2011) 2359–2370, https://doi.org/10.1002/app.32650.

[227] C.S. Bentivoglio Ruiz, L.D.B. Machado, J.E. Volponi, E. Segura Pino, Oxygen inhibition and coating thickness effects on Uv radiation curing of weatherfast clearcoats studied by photo-DSC, J. Therm. Anal. Calorim. 75 (2004) 507–512, https://doi.org/10.1023/B:JTAN.0000027140.27560.d1.

[228] A. Tiwari, A. Polykarpov (Eds.), Photocured materials, Royal Society of Chemistry RSC Publ, Cambridge, 2015.

[229] E. Andrzejewska, M.B. Bogacki, M. Andrzejewski, M. Janaszczyk, Termination mechanism during the photo-induced radical cross-linking polymerization in the presence and absence of oxygen, Phys. Chem. Chem. Phys. 5 (2003) 2635, https://doi.org/10.1039/b301849k.

[230] K. Studer, C. Decker, E. Beck, R. Schwalm, Overcoming oxygen inhibition in UV-curing of acrylate coatings by carbon dioxide inerting: Part II, Prog. Org. Coat. 48 (2003) 101–111, https://doi.org/10.1016/S0300-9440(03)00149-8.

[231] S.C. Ligon, B. Husár, H. Wutzel, R. Holman, R. Liska, Strategies to reduce oxygen inhibition in photoinduced polymerization, Chem. Rev. 114 (2014) 557–589, https://doi.org/10.1021/cr3005197.

[232] J.-T. Lin, H.-W. Liu, K.-T. Chen, D.-C. Cheng, Modeling the kinetics, curing depth, and efficacy of radical-mediated photopolymerization: the role of oxygen inhibition, viscosity, and dynamic light intensity, Front. Chem. 7 (2019) 760, https://doi.org/10.3389/fchem.2019.00760.

[233] A.K. O'Brien, C.N. Bowman, Impact of oxygen on photopolymerization kinetics and polymer structure, Macromolecules 39 (2006) 2501–2506, https://doi.org/10.1021/ma051863l.

[234] C. Decker, A.D. Jenkins, Kinetic approach of oxygen inhibition in ultraviolet- and laser-induced polymerizations, Macromolecules 18 (1985) 1241–1244, https://doi.org/10.1021/ma00148a034.

[235] J. Christmann, C. Ley, X. Allonas, A. Ibrahim, C. Croutxé-Barghorn, Experimental and theoretical investigations of free radical photopolymerization: Inhibition and termination reactions, Polymer 160 (2019) 254–264, https://doi.org/10.1016/j.polymer.2018.11.057.

[236] A.S. Jariwala, F. Ding, A. Boddapati, V. Breedveld, M.A. Grover, C.L. Henderson, D.W. Rosen, Modeling effects of oxygen inhibition in mask-based stereolithography, Rapid Prototyp. J. 17 (2011) 168–175, https://doi.org/10.1108/13552541111124734.

[237] A.K. O'Brien, C.N. Bowman, Modeling the effect of oxygen on photopolymerization kinetics, Macromol. Theory Simul. 15 (2006) 176–182, https://doi.org/10.1002/mats.200500056.

[238] N. Caiger, S. Herlihy, Oxygen inhibition effects in UV-Curing Inkjet Inks, S T Soc. Imaging Sci. Technol. (1999) 116–119.

[239] Z. Zhao, X. Mu, J. Wu, H.J. Qi, D. Fang, Effects of oxygen on interfacial strength of incremental forming of materials by photopolymerization, Extrem. Mech. Lett. 9 (2016) 108–118, https://doi.org/10.1016/j.eml.2016.05.012.

[240] S.K. Kim, C.A. Guymon, Effects of polymerizable organoclays on oxygen inhibition of acrylate and thiol-acrylate photopolymerization, Polymer 53 (2012) 1640–1650, https://doi.org/10.1016/j.polymer.2012.02.028.

[241] D. Ahn, L.M. Stevens, K. Zhou, Z.A. Page, Additives for ambient 3D printing with visible light, Adv. Mater. (Deerfield Beach, Fla.) 33 (2021), https://doi.org/10.1002/adma.202104906.

[242] O. Llorente, A. Agirre, I. Calvo, M. Olaso, R. Tomovska, H. Sardon, Exploring the advantages of oxygen-tolerant thiol-ene polymerization over conventional acrylate free radical photopolymerization processes for pressure-sensitive adhesives, Polym. J. 53 (2021) 1195–1204, https://doi.org/10.1038/s41428-021-00520-z.

[243] F.R. Wight, I.M. Nunez, Oxygen inhibition of acrylate photopolymerization, J. Radiat. Curing 16 (1989) 3–8.

[244] C. Schmitz, T. Poplata, A. Feilen, B. Strehmel, Radiation crosslinking of pigmented coating material by UV LEDs enabling depth curing and preventing oxygen inhibition, Prog. Org. Coat. 144 (2020), 105663, https://doi.org/10.1016/j.porgcoat.2020.105663.

[245] J.-T. Lin, D.-C. Cheng, K.-T. Chen, Y.-C. Chiu, H.-W. Liu, Enhancing UV photopolymerization by a red-light preirradiation: kinetics and modeling strategies for reduced oxygen inhibition, J. Polym. Sci. 58 (2020) 683–691, https://doi.org/10.1002/pol.20190201.

[246] J.-T. Lin, K.-T. Chen, P.-K. Chang, D.-C. Cheng, Enhancing blue-light-initiated photopolymerization in a three-component system: kinetic and modeling of conversion strategies, J. Polym. Res 28 (2021), https://doi.org/10.1007/s10965-020-02398-6.

[247] K. Taki, R. Yamada, Comparison of the degree of shrinkage under air and nitrogen atmospheres by laser displacement sensor, J. Photo Sci. Technol. 31 (2018) 497–501, https://doi.org/10.2494/photopolymer.31.497.

[248] K. Studer, C. Decker, E. Beck, R. Schwalm, Overcoming oxygen inhibition in UV-curing of acrylate coatings by carbon dioxide inerting, part I, Prog. Org. Coat. 48 (2003) 92–100, https://doi.org/10.1016/S0300-9440(03)00120-6.

[249] H. Gojzewski, Z. Guo, W. Grzelachowska, M.G. Ridwan, M.A. Hempenius, D. W. Grijpma, G.J. Vancso, Layer-by-layer printing of photopolymers in 3D: how weak is the interface? ACS Appl. Mater. Interfaces 12 (2020) 8908–8914, https://doi.org/10.1021/acsami.9b22272.

[250] W.R. Smith, Q. Wang, A theoretical model for the growth of spherical bubbles by rectified diffusion, J. Fluid Mech. 939 (2022), https://doi.org/10.1017/jfm.2022.218.

[251] R. Jeurissen, J. de Jong, H. Reinten, M. van den Berg, H. Wijshoff, M. Versluis, D. Lohse, Effect of an entrained air bubble on the acoustics of an ink channel, J. Acoust. Soc. Am. 123 (2008) 2496–2505, https://doi.org/10.1121/1.2835624.

[252] P. He, B. Derby, Controlling coffee ring formation during drying of inkjet printed 2D inks, Adv. Mater. Interfaces 4 (2017), 1700944, https://doi.org/10.1002/admi.201700944.

[253] X. Yu, R. Xing, Z. Peng, Y. Lin, Z. Du, J. Ding, L. Wang, Y. Han, To inhibit coffee ring effect in inkjet printing of light-emitting polymer films by decreasing capillary force, Chin. Chem. Lett. 30 (2019) 135–138, https://doi.org/10.1016/j.cclet.2018.09.007.

[254] E. Sowade, M. Polomoshnov, A. Willert, R.R. Baumann, Toward 3D-printed electronics: inkjet-printed vertical metal wire interconnects and screen-printed batteries, Adv. Eng. Mater. 21 (2019), 1900568, https://doi.org/10.1002/adem.201900568.

[255] L.-W. Lo, H. Shi, H. Wan, Z. Xu, X. Tan, C. Wang, Inkjet-printed soft resistive pressure sensor patch for wearable electronics applications, Adv. Mater. Technol. 5 (2020), 1900717, https://doi.org/10.1002/admt.201900717.

[256] M.J. Griffith, N.A. Cooling, D.C. Elkington, M. Wasson, X. Zhou, W.J. Belcher, P. C. Dastoor, Controlling nanostructure in inkjet printed organic transistors for pressure sensing applications, Nanomaterials 11 (2021) 1185, https://doi.org/10.3390/nano11051185.

[257] H. Jeong, Y. Cui, M.M. Tentzeris, S. Lim, Hybrid (3D and inkjet) printed electromagnetic pressure sensor using metamaterial absorber, Addit. Manuf. 35 (2020), 101405, https://doi.org/10.1016/j.addma.2020.101405.

[258] Y. Chu, C. Qian, P. Chahal, C. Cao, Printed diodes: materials processing, fabrication, and applications, Adv. Sci. 6 (2019), 1801653, https://doi.org/10.1002/advs.201801653.

[259] S. Singh, H. Matsui, S. Tokito, Printed dual-gate organic thin film transistors and PMOS inverters on flexible substrates: role of top gate electrode, J. Phys. D: Appl. Phys. 55 (2022), 135105, https://doi.org/10.1088/1361-6463/ac44c2.

[260] B. Park, J. Jang, H. Kim, J. Seo, H. Yoo, T. Kim, Y. Hong, Enhanced current path by circularly and periodically-aligned semiconducting single-walled carbon nanotubes for logic circuit device, Flex. Print. Electron. 7 (2022) 15005, https://doi.org/10.1088/2058-8585/ac4ea0.

[261] T.N. Mangoma, S. Yamamoto, G.G. Malliaras, R. Daly, Hybrid 3D/inkjet-printed organic neuromorphic transistors, Adv. Mater. Technol. 7 (2022), 2000798, https://doi.org/10.1002/admt.202000798.

[262] P. Oser, J. Jehn, M. Kaiser, O. Düttmann, F. Schmid, L. Schulte-Spechtel, S. S. Rivas, C. Eulenkamp, C. Schindler, C.U. Grosse, D. Wu, Fiber-optic photoacoustic generator realized by inkjet-printing of CNT-PDMS composites on fiber end faces, Macromol. Mater. Eng. 306 (2021), 2000563, https://doi.org/10.1002/mame.202000563.

[263] L. Zhang, D. Chao, P. Yang, L. Weber, J. Li, T. Kraus, H.J. Fan, Flexible pseudocapacitive electrochromics via inkjet printing of additive-free tungsten oxide nanocrystal ink, Adv. Energy Mater. 10 (2020), 2000142, https://doi.org/10.1002/aenm.202000142.

[264] Y. Bräuniger, S. Lochmann, J. Grothe, M. Hantusch, S. Kaskel, Piezoelectric inkjet printing of nanoporous carbons for micro-supercapacitor devices, ACS Appl. Energy Mater. 4 (2021) 1560–1567, https://doi.org/10.1021/acsaem.0c02745.

[265] F. Schackmar, H. Eggers, M. Frericks, B.S. Richards, U. Lemmer, G. Hernandez-Sosa, U.W. Paetzold, Perovskite solar cells with all-inkjet-printed absorber and charge transport layers, Adv. Mater. Technol. 6 (2021), 2000271, https://doi.org/10.1002/admt.202000271.

[266] C. Wei, W. Su, J. Li, B. Xu, Q. Shan, Y. Wu, F. Zhang, M. Luo, H. Xiang, Z. Cui, H. Zeng, A. Universal Ternary-Solvent-Ink, Strategy toward efficient inkjet-printed perovskite quantum dot light-emitting diodes, Adv. Mater. 34 (2022), e2107798, https://doi.org/10.1002/adma.202107798.

[267] L. Shi, L. Meng, F. Jiang, Y. Ge, F. Li, X. Wu, H. Zhong, In situ inkjet printing strategy for fabricating perovskite quantum dot patterns, Adv. Funct. Mater. 29 (2019), 1903648, https://doi.org/10.1002/adfm.201903648.

[268] Y.J. Donie, S. Schlisske, R.H. Siddique, A. Mertens, V. Narasimhan, F. Schackmar, M. Pietsch, I.M. Hossain, G. Hernandez-Sosa, U. Lemmer, G. Gomard, Phase-separated nanophotonic structures by inkjet printing, ACS Nano 15 (2021) 7305–7317, https://doi.org/10.1021/acsnano.1c00552.

[269] J. Kimionis, A. Georgiadis, M. Isakov, H.J. Qi, M.M. Tentzeris, 3D/inkjet-printed origami antennas for multi-direction RF harvesting, in: 2015 IEEE MTT-S International Microwave Symposium (IMS 2015), Phoenix, AZ, USA, IEEE, Piscataway, NJ, 2015, pp. 1–4.

[270] A. Rida, L. Yang, R. Vyas, M.M. Tentzeris, Conductive inkjet-printed antennas on flexible low-cost paper-based substrates for rfid and wsn applications, IEEE Antennas Propag. Mag. 51 (2009) 13–23, https://doi.org/10.1109/MAP.2009.5251188.

[271] S.F. Jilani, Q.H. Abbasi, A. Alomainy, Inkjet-Printed Millimetre-Wave PET-Based Flexible Antenna for 5G Wireless Applications, Dublin, IEEE, 30.08.2018 - 31.08.2018, pp. 1–3.

[272] D. Mitra, R. Thalheim, R. Zichner, Inkjet printed heating elements based on nanoparticle silver ink with adjustable temperature distribution for flexible applications, Phys. Status Solidi A 218 (2021), 2100257, https://doi.org/10.1002/pssa.202100257.

[273] J. Koo, J.W. Kim, M. Kim, S. Yoon, J.H. Shim, Inkjet printing of silica aerogel for fabrication of 2-D patterned thermal insulation layers, Int. J. Precis. Eng. Manuf. - Green. Technol. 8 (2021) 445–451, https://doi.org/10.1007/s40684-020-00189-4.

[274] J. Abu-Khalaf, R. Saraireh, S. Eisa, A. Al-Halhouli, Experimental characterization of inkjet-printed stretchable circuits for wearable sensor applications, Sensors 18 (2018) 3476, https://doi.org/10.3390/s18103476.

[275] S. Seipel, J. Yu, A.P. Periyasamy, M. Viková, M. Vik, V.A. Nierstrasz, Inkjet printing and UV-LED curing of photochromic dyes for functional and smart textile applications, RSC Adv. 8 (2018) 28395–28404, https://doi.org/10.1039/C8RA05856C.

[276] M.J. Park, C. Wang, D.H. Seo, R.R. Gonzales, H. Matsuyama, H.K. Shon, Inkjet printed single walled carbon nanotube as an interlayer for high performance thin film composite nanofiltration membrane, 0376–7388 (2021). https://doi.org/10.1016/j.memsci.2020.118901.

[277] A. Banquart, S. Callé, F. Levassort, L. Fritsch, F. Ossant, S. Toffessi Siewe, S. Chevalliot, A. Capri, J.-M. Grégoire, Piezoelectric P(VDF-TrFE) film inkjet printed on silicon for high-frequency ultrasound applications, J. Appl. Phys. 129 (2021), 195107, https://doi.org/10.1063/5.0048444.

[278] H. Kang, J.W. Lee, Y. Nam, Inkjet-Printed Multiwavelength Thermoplasmonic Images For Anticounterfeiting Applications, ACS Appl. Mater. Interfaces 10 (2018) 6764–6771, https://doi.org/10.1021/acsami.7b19342.

[279] R. Shanker, S. Sardar, S. Chen, S. Gamage, S. Rossi, M.P. Jonsson, NoniridescEnt Biomimetic Photonic Microdomes By Inkjet Printing, Nano Lett. 20 (2020) 7243–7250, https://doi.org/10.1021/acs.nanolett.0c02604.

[280] J. Sun, C. Yun, B. Cui, P. Li, G. Liu, X. Wang, F. Chu, A Facile Approach For Fabricating Microstructured Surface Based On Etched Template By Inkjet Printing Technology, Polymers 10 (2018), https://doi.org/10.3390/polym10111209.

[281] Y. Cui, S.A. Nauroze, R. Bahr, M.M. Tentzeris, A. Novel Additively 4D Printed Origami-inspired Tunable Multi-layer Frequency Selective Surface for mm-Wave IoT, RFID, WSN, 5G, and Smart City Applications, in: 2021 IEEE MTT-S International Microwave Symposium (IMS), Atlanta, GA, USA, IEEE, 2021, pp. 86–89.

[282] V.K. Chatziiona, B.K. Constantinou, P.G. Savva, G.G. Olympiou, K. Kapnisis, A. Anayiotos, C.N. Costa, Regulating the catalytic properties of Pt/Al2O3 through nanoscale inkjet printing 1566–7367 (103) (2018) 69–73, https://doi.org/10.1016/j.catcom.2017.09.016.

[283] A. Willert, F.Z. Tabary, T. Zubkova, P.E. Santangelo, M. Romagnoli, R. R. Baumann, Multilayer additive manufacturing of catalyst-coated membranes for polymer electrolyte membrane fuel cells by inkjet printing, Int. J. Hydrog. Energy 47 (2022) 20973–20986, https://doi.org/10.1016/j.ijhydene.2022.04.197.

[284] H. Maleki, V. Bertola, Recent advances and prospects of inkjet printing in heterogeneous catalysis, Catal. Sci. Technol. 10 (2020) 3140–3159, https://doi.org/10.1039/D0CY00040J.

[285] P. Kumar, S. Ebbens, X. Zhao, Inkjet printing of mammalian cellS – Theory and applications, Bioprinting 23 (2021), e00157, https://doi.org/10.1016/j.bprint.2021.e00157.

[286] Nanodimension, Nano Dimension Disrupts Printed Electronics with World's First 3D Printer Dedicated to Ultra-Rapid Prototyping of PCBs. ⟨https://www.nano-di.com/newsroom/nano-dimension-disrupts-printed-electronics-with-worlds-first-3d-printer-dedicated-to-ultra-rapid-prototyping-of-pcbs⟩ (accessed 11 October 2022).

[287] L.M. Kuhnke, J.S. Rehfeld, C. Ude, S. Beutel, Study on the development and integration of 3D-printed optics in small-scale productions of single-use cultivation vessels, Eng. life Sci. 22 (2022) 440–452, https://doi.org/10.1002/elsc.202100131.

[288] G.L. Duffy, H. Liang, R.L. Williams, D.A. Wellings, K. Black, 3D reactive inkjet printing of poly-ε-lysine/gellan gum hydrogels for potential corneal constructs, Mater. Sci. Eng. C., Mater. Biol. Appl. 131 (2021), 112476, https://doi.org/10.1016/j.msec.2021.112476.

[289] L.B. Bezek, C.A. Chatham, D.A. Dillard, C.B. Williams, Mechanical properties of tissue-mimicking composites formed by material jetting additive manufacturing, J. Mech. Behav. Biomed. Mater. 125 (2022), 104938, https://doi.org/10.1016/j.jmbbm.2021.104938.

[290] R. Walczak, B. Kawa, K. Adamski, Inkjet 3D printed microfluidic device for growing seed root and stalk mechanical characterization, Sens. Actuators A Phys. 297 (2019), 111557, https://doi.org/10.1016/j.sna.2019.111557.

[291] R. Walczak, K. Adamski, W. Kubicki, Inkjet 3D printed modular microfluidic chips for on-chip gel electrophoresis, J. Micromech. Micro 29 (2019) 57001, https://doi.org/10.1088/1361-6439/ab0e64.

[292] K. Adamski, B. Kawa, R. Walczak, Inkjet 3D Printed Venturi Microflowmeter. 2018 XV International Scientific Conference on Optoelectronic and Electronic Sensors (COE), IEEE, Warsaw, Poland, 2018, pp. 1–3.

[293] A.R. Bhatti, M. Mott, J.R.G. Evans, M.J. Edirisinghe, PZT pillars for 1-3 composites prepared by ink-jet printing, J. Mater. Sci. Lett. 20 (2001) 1245–1248, https://doi.org/10.1023/A:1010987209703.

[294] X. Zhao, J.R.G. Evans, M.J. Edirisinghe, J.H. Song, Ink-jet printing of ceramic pillar arrays, J. Mater. Sci. 37 (2002) 1987–1992, https://doi.org/10.1023/A:1015247131016.

[295] S. Kriegseis, L. Aretz, M.-E. Jennes, F. Schmidt, T. Tonnesen, K. Schickle, 3D printing of complex ceramic dental implant abutments by using Direct Inkjet Printing, Mater. Lett. 313 (2022), 131789, https://doi.org/10.1016/j.matlet.2022.131789.

[296] L.A. Junqueira, A.G. Tabriz, F.J. Raposo, L.R. Carobini, U.P. Vaz, M.A.F. Brandão, D. Douroumis, N.R.B. Raposo, CoupliNg of fused deposition modeling and inkjet printing to produce drug loaded 3D printed tablets, Pharmaceutics 14 (2022), https://doi.org/10.3390/pharmaceutics14010159.

[297] D.J. Roach, C. Roberts, J. Wong, X. Kuang, J. Kovitz, Q. Zhang, T.G. Spence, H. J. Qi, Surface modification of fused filament fabrication (FFF) 3D printed substrates by inkjet printing polyimide for printed electronics, Addit. Manuf. 36 (2020), 101544, https://doi.org/10.1016/j.addma.2020.101544.

[298] S. Anelli, M. Rosa, F. Baiutti, M. Torrell, V. Esposito, A. Tarancón, Hybrid-3D printing of symmetric solid oxide cells by inkjet printing and robocasting, Addit. Manuf. 51 (2022), 102636, https://doi.org/10.1016/j.addma.2022.102636.

[299] K. Picha, C. Spackman, J. Samuel, Droplet spreading characteristics observed during 3D printing of aligned fiber-reinforced soft composites, Addit. Manuf. 12 (2016) 121–131, https://doi.org/10.1016/j.addma.2016.08.004.

[300] T. Stäbler, K. Chen, T. Cziep, M. Echsel, M. Ehresmann, J. Fischer, L. Friedrich, M. Fugmann, D. Galla, N. Gottschalk, J. Hildebrandt, S. Hümbert, J. Skalden, T. Stindl, IRAS -new technologies for low cost satellites, in: Conference: 72 nd International Astronautical Congress, UAE, Dubai, 2021.

[301] M.J. Mirzaali, A.H. de La Nava, D. Gunashekar, M. Nouri-Goushki, E. L. Doubrovski, A.A. Zadpoor, Fracture behavior of bio-inspired functionally graded soft-hard composites made by multi-material 3D printing: the case of colinear cracks, Materials 12 (2019), https://doi.org/10.3390/ma12172735.

[302] E. Salcedo, D. Baek, A. Berndt, J.E. Ryu, Simulation and validation of three dimension functionally graded materials by material jetting, Addit. Manuf. 22 (2018) 351–359, https://doi.org/10.1016/j.addma.2018.05.027.

[303] N.A. Meisel, D.A. Dillard, C.B. Williams, Impact of material concentration and distribution on composite parts manufactured via multi-material jetting, Rapid Prototyp. J. 24 (2018) 872–879, https://doi.org/10.1108/RPJ-01-2017-0005.

[304] L. Zorzetto, L. Andena, F. Briatico-Vangosa, L. Noni, J.-M. Thomassin, C. Jérôme, Q. Grossman, A. Mertens, R. Weinkamer, M. Rink, D. Ruffoni, Properties and role of interfaces in multimaterial 3D printed composites, Sci. Rep. 10 (2020) 22285, https://doi.org/10.1038/s41598-020-79230-0.

[305] Y.-L. Cheng, K.-C. Huang, Preparation and characterization of color photocurable resins for full-color material jetting additive manufacturing, Polymers 12 (2020), https://doi.org/10.3390/polym12030650.

[306] M. Hašan, M. Fuchs, W. Matusik, H. Pfister, S. Rusinkiewicz, Physical reproduction of materials with specified subsurface scattering, ACM Trans. Graph. 29 (2010) 1–10, https://doi.org/10.1145/1778765.1778798.

[307] T.S. Lumpe, J. Mueller, K. Shea, Tensile properties of multi-material interfaces in 3D printed parts, Mater. Des. 162 (2019) 1–9, https://doi.org/10.1016/j.matdes.2018.11.024.

[308] J.P. Moore, C.B. Williams, Fatigue characterization of 3D printed elastomer material, Austin, TX, University of Texas at Austin (freeform), Austin, TX, 2012, pp. 641–655.

[309] I. Raza, L. Iannucci, P.T. Curtis, Introducing a multimaterial printer for the deposition of low melting point alloys, elastomer, and ultraviolet curable resin, 3D Print. Addit. Manuf. 4 (2017) 83–89, https://doi.org/10.1089/3dp.2016.0053.